III. ENVIRONMENTAL ISSUES

HARMFUL ALGAL BLOOMS IN THE OCEAN: AN EXAMPLE TO INTRODUCE HIGH SCHOOL STUDENTS TO ENVIRONMENTAL PROBLEMS

Ulrike Feudel
Institute for Chemistry and Biology of the Marine Environment, Carl von Ossietzky University, Oldenburg, Germany, ulrike.feudel@uni-oldenburg.de

ABSTRACT

Tackling problems in environmental science needs an interdisciplinary approach in which physics, chemistry and biology are coupled to address the impact of global change on processes in atmosphere, oceans and biosphere. Using simple conceptual models of populations we demonstrate (i) the complexity of the dynamics which can arise due to changes in the environment and (ii) how to analyze the problem of the formation of harmful algal blooms in the ocean. Furthermore, we show how methods from theoretical physics can be utilized to model ecological processes.

INTRODUCTION

School education is mostly devoted to the different science subjects like physics, chemistry and biology taught independently of each other. However, most major problems in climate and environmental science require the intimate interplay between different disciplines to understand e.g. the impact of changes in the physical environment like global warming on ecosystems. For this reason it would be most appreciated if already at the school level one would start demonstrating with simple models how important questions in environmental science can be tackled combining different disciplines of science. Here we will give a short introduction into some phenomena in ecosystem dynamics, particularly in marine science. We use methods borrowed from physics to set up the model and to analyse it. Furthermore we show how the physical environment influences the dynamics of the biological system.

Phytoplankton are organisms living in all oceans, rivers and lakes and can be considered as plants since they produce organic material from inorganic nutrients utilizing sunlight for photosynthesis. Moreover, phytoplankton constitutes the base of the aquatic food web [1] and produces more than half of the oxygen in the world [2]. Furthermore, it is an integral part of the global carbon cycle [3] and plays, hence, a major role in climate dynamics. Changes in phytoplankton dynamics would thus have major consequences for mankind. Due to seasonal changes in temperature and light conditions, i.e. the physical conditions in the environment, phytoplankton species develop large abundances called algal blooms mostly in spring and some also in the autumn. Such blooms, in turn, trigger the growth of species at higher trophic levels like zooplankton and fish, which feed upon phytoplankton. The phenomena, which we would like to address here specifically, are so-called harmful algal blooms that are caused by species, which are e.g. capable of producing harmful substances supressing the growth of competitors and predators or even leading to their death due to the toxicity of those substances. Besides the toxic substances can accumulate in predators and finally be transferred to organisms on higher trophic levels like fish and humans. Therefore, harmful algal blooms may cause large economic losses due to their threat to fish farming and the health of people. Moreover they have a severe impact on ecosystem dynamics.

To gain some insight into the formation of harmful algal blooms, we will firstly discuss briefly the main steps of modelling in science with particular emphasis on models in ecology. This methodology is based on the theory of nonlinear dynamical systems. Next, we will demonstrate that even in rather simple population models the dynamics can be rather complex and discuss the limits of predictability. Finally we analyse a particular model of harmful algal blooms to illustrate how changes in the environment influence the emergence of harmful algal blooms. Using these simple illustrations one can get school students interested in modelling environmental problems.

MODELLING ECOLOGICAL DYNAMICS

Dynamical systems are frequently used to study various phenomena from diverse disciplines of science such as laser physics, population ecology, socioeconomic studies, and many others. The corresponding mathematical models are often formulated in terms of balance equations, in which the time evolution of the state variables is determined by possibly several gain and loss terms. In the modeling process the modeler usually decides first which processes are important and need to be included in the model and second, which specific mathematical function describes best those processes and reflects either empirical evidence or some theoretical reasoning. In this way a specific model for the phenomenon under consideration is constructed.

When constructing models in physics one begins usually from the first principles like e.g. Newton's laws in mechanics. However, in ecology such first principles are not available and the modeler has to formulate mathematical functions for processes like growth, competition, predator-prey interactions like grazing or death. In literature several such formulations are provided which fulfill some basic biological features. To illustrate the obtained dynamics we discuss here the formulation of growth as well as predator-prey dynamics.

In the simplest form the growth of a species X is modeled using a constant growth rate *r* of an individual which is multiplied by its abundance leading to an overall growth term $dX/dt=rX$. This formulation would lead to an exponential growth $X(t)=X(0)exp(rt)$, which is rather unrealistic since it does not take into account, that resources as a necessary input for growth are in general limited and individuals will compete for these resources. If one also considers this limitation, then one has to include a term for the competition, which can be expressed as a quadratic term in the abundances of the species *X*. This formulation results in a differential equation containing one gain term, the growth, and one loss term, the competition for the constant resource *K*, called carrying capacity:

$$\frac{\mathrm{dX}}{dt} = rX\left(1-\frac{\mathrm{X}}{K}\right) \tag{1}$$

The dynamics of this limited growth leads to a constant equilibrium in which the gain balances the losses resulting in an abundance of the species, which equals the carrying capacity. A growth described in this form is called logistic growth [4].

This situation changes if the model does not describe a system in which the time is continuous, but discrete [5]. Such population models represent species, which have a yearly breeding cycle like insects and birds and in which the number of individuals is counted each year at approximately the same time. The corresponding dynamics can be expressed in terms of a map in which the index i denotes the year in which the population is considered:

$$X_{i+1} = rX_i\left(1-\frac{\mathrm{X_i}}{K}\right) \quad . \tag{2}$$

The complexity of the dynamics in this model depends strongly on the value of the growth rate *r* (cf. Fig.1, upper panel). For a small growth rate, we obtain either a fixed point, in which the population does not change over the years or periodic behavior with different periods. For larger growth rate we obtain chaotic behavior in which it is impossible to predict the abundance of the population of species *X* in the next year. Though this model is rather simple, it possesses for certain growth rates a very complex irregular dynamics as depicted in Fig.1. (lower panel). This chaotic behavior limits the predictability of the system, since initially nearby trajectories diverge exponentially.

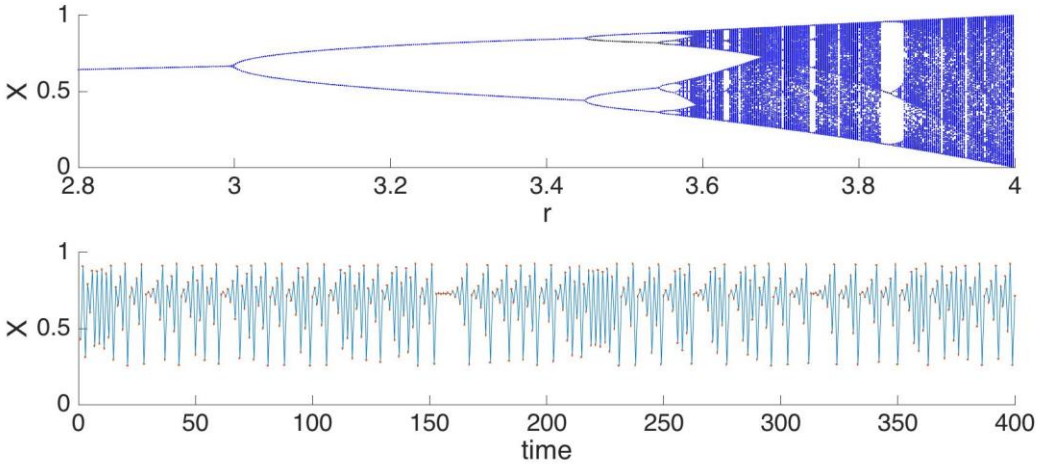

Fig.1. Discrete dynamics of a population restricted by limited resources described by the logistic map with carrying capacity K=1. Upper panel: Dynamics depending on the growth rate r. Lower panel: Time evolution of the population abundance in the chaotic parameter region, here computed at r=3.7.

As another example for modeling ecological processes, we mention predator-prey interactions, where the growth rate of the predator depends on the abundance of a prey called *X*. The formulation of the uptake or grazing rate has to fulfill certain biological empirical evidence. The grazing rate *f(X)* has to be zero if no prey is available, i.e. *f(0)=0*. Then it should grow with increasing prey availability, but finally saturate since the predator can eat only a certain amount of prey regardless of the number of prey species in case they are highly abundant. This would be well described by a function which is monotonously increasing for small values of *X* but finally go to a constant for large *X*. As an illustration we show in Fig.2 the mostly used mathematical formulations of the grazing rates of a predator depending on the prey [6].

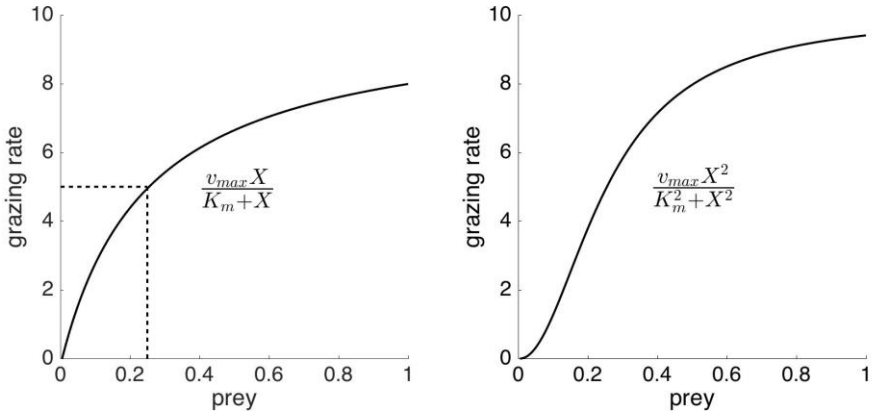

Fig.2. Different types of predator-prey interactions: Left panel: Holling type II, the dashed line indicates the line at which the prey abundance is equal to K_m and the grazing rate equals the maximum grazing rate v_{max}. Right panel: Holling type III

Depending on the complexity of the processes taken into account, these functions can be rather simple as described above or more complicated if e.g. the behavior of organisms like different hunting strategies depending on prey availability is additionally taken into account.

MODELLING HARMFUL ALGAL BLOOMS (HABS)

As already mentioned in the introduction harmful algal blooms constitute a major problem in many regions of the world's oceans. While there is an annual bloom of non-harmful species in spring, HABs occur either sporadically or if they appear on a regular annual basis, their magnitude, the exact timing of their onset, their specific location and geographical extent, their composition (i.e. which species dominates) as well as their duration and termination vary significantly from year to year. Therefore it is necessary to understand the mechanisms leading to triggering such harmful blooms in order to predict them. Several physical, chemical and biological factors are believed to contribute to the specific conditions under which HABs develop [7]. Moreover, climate change has led to a substantial increase in the number of HABs around the globe [8]. Possible causes for this increase are increasing input of nutrients into the oceans due to fertilizers used in agriculture and their subsequent transport into the ocean by river run-off, the warming of the ocean, changes in hydrodynamic flows due to climate change as well as the invasion of new species.

Several conceptual, empirical and numerical models have been developed to understand the main trigger mechanisms of harmful algal blooms [9, 10]. The complexity of those models depends on the number of processes and influencing physical and biological factors taken into account. We will focus here only on one model, which is particularly simple and can therefore be studied by high school students. Truscott and Brindley [11] formulated a model, which considers only the interaction between the harmful phytoplankton species as a prey and zooplankton as its predator. The mathematical functions taken into account for predator-prey interactions allow to explain dynamics as a nonlinear "excitable system". This model has been used to study red tides, i.e. HABs that are caused by a particular species, which changes the ocean color into red if they are very abundant. Excitability means here that a system which is usually in equilibrium is capable of developing a huge response in the form of a pulse when it is perturbed with a certain perturbation. A typical example for an excitable system is the excitation of a neuron, when it gets some input signal. The resulting dynamics consists of a fast growth of the so-called excitatory variable followed by a slower growth of the inhibitory variable. When the inhibitory variable is large enough, it starts suppressing the excitatory variable resulting in the end of the excitation and a return to the equilibrium.

The underlying model for a harmful algal bloom consists of two differential equations for phytoplankton *P* as prey and zooplankton *Z* as predator respectively:

$$\frac{dP}{dt} = r \cdot P \cdot \left(1 - \frac{P}{K}\right) - \alpha \cdot \frac{P^2}{\mu^2 + P^2} \cdot Z$$
$$\frac{dZ}{dt} = \gamma \cdot \alpha \cdot \frac{P^2}{\mu^2 + P^2} \cdot Z - d \cdot Z \qquad (3)$$

The first term in the phytoplankton equation describes the logistic growth of the phytoplankton with a rate *r* taking into the competition of phytoplankton cells for the limited resource K. The second term denotes the grazing of zooplankton cells upon phytoplankton. The grazing rate is modeled as an S-shaped Holling-type III function (cf. Fig. 2), i.e. it is very slowly increasing when prey is scarce, but then it is increasing quadratic with prey abundance until it saturates for large prey abundance. The time evolution of the zooplankton abundance is also formulated in terms of a balance equation in which the gain in zooplankton abundance is almost equal to the grazing term except for a prefactor γ which measures how much of the prey taken up is converted into predator biomass. The natural mortality of zooplankton – the last term in the zooplankton equation – is modeled with a rate *d*.

To illustrate the excitable dynamics we show in Fig.3. the time evolution of the response of phytoplankton and zooplankton after applying a perturbation in the zooplankton concentration. Truscott and Brindley [11] found that a zooplankton concentration below some critical level helps to bring the system into an "excited" state thereby initiating a bloom of phytoplankton. In the terminology of excitable systems, phytoplankton is the excitatory variable while zooplankton feeding upon it is the inhibitory variable.

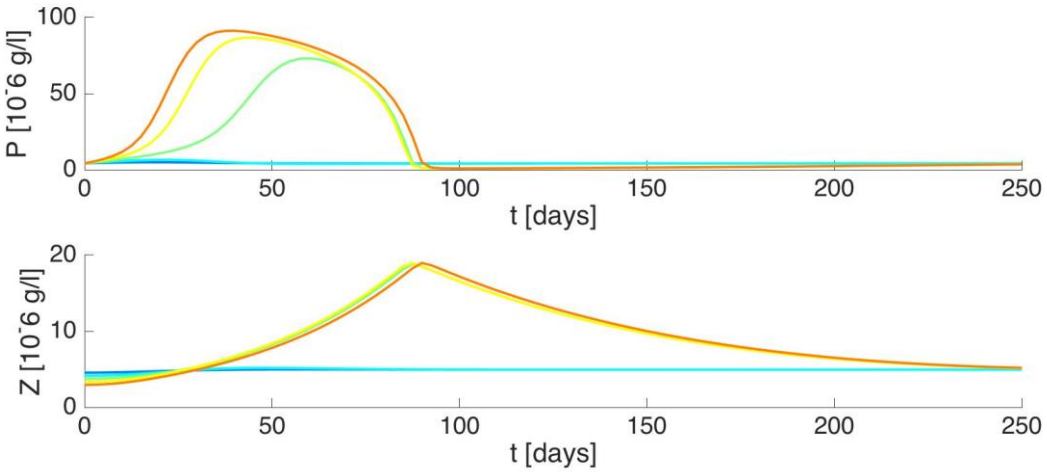

Fig.3: Time evolution of the Truscott-Brindley model, Eqs.(3), for different initial concentrations of zooplankton *Z*. Only low initial concentrations of zooplankton (orange, yellow and green curves) lead to a large response of phytoplankton *P*. The parameters for this simulation are: r = 0.3 day^{-1}, K = 108 g/l, α = 0.7 day^{-1}, μ = 5.7 g/l, d = 0.012 day^{-1}, γ = 0.05.

Let us now discuss the impact of the physical environment on the emergence of such harmful algal blooms. Two different important physical factors are considered in the following: temperature and hydrodynamic flows. While temperature influences the growth rates of plankton, hydrodynamic flows are responsible for the redistribution of nutrients and plankton in the water.

The growth of plankton depends crucially on the seasonal cycle. While in winter plankton abundance is low, it starts growing in spring when temperature and light availability are increasing. To take this factor into account, we introduce the temperature dependence of the growth rate via a factor, which scales the growth rate *r* based on the Arrhenius law as

$$r(T) = r \cdot Q_{10}^{(T-\bar{T})/10} \tag{4}$$

where Q_{10} is a species-dependent constant factor. This scaling means that a change in temperature by 10^o multiplies the growth rate by the factor Q_{10}. The temperature T varies with the seasonal cycle having a period of 365 days.

$$T(t) = \bar{T} + \Delta T \cos(\Omega t + \varphi) \tag{5}$$

Simulating the dynamics of the plankton model yields now a periodic behavior instead of the equilibrium we obtained before. When different initial abundances for the two species are selected we note that two different behaviors are possible: either we find a year in which no harmful bloom occurs or a strong harmful bloom develops (Fig. 4). This result reveals that we have two coexisting alternative states, years with and without blooms. Based on this finding we can explain the irregular bloom behavior observed in nature: When we consider a periodic temperature influence, that is equal each year, both, bloom and non-bloom dynamics are possible depending on the initial conditions. However, the temperature is only on average the same every year. In reality, small variations in temperature occur each year, so that the temperature on, say June 1, is not each year the same but possesses small fluctuations, which are caused by the weather patterns, which vary from year to year. Taking these fluctuations into account, the system is able to switch from non-bloom to bloom years and vice versa. This irregular switching resembles the dynamics of harmful blooms in nature [12].

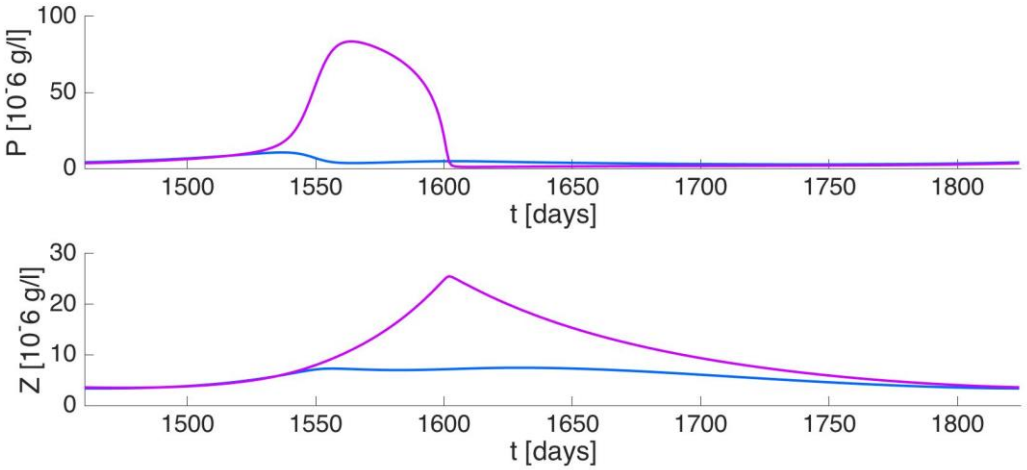

Fig.4. Abundances for phytoplankton (upper panel) and zooplankton (lower panel) for two different initial abundances: non-bloom year (blue), bloom year (magenta). Parameters are the same as in Fig. 3, $\Omega = 2\pi/365$ day^{-1}, T = 10^o, $\Delta T=6^o$, $\Phi = 0.59$.

Plankton blooms develop in the water column and are transported together with the inorganic nutrients – their food – by hydrodynamic flows. It is important to note, that hydrodynamic flows have in general very different time scales than biological processes. While the growth of plankton is on a time scale of days to weeks, ocean flow pattern travel in this time interval several hundreds of kilometers. To obtain an impact of flow patterns on plankton blooms one has to look for coherent structures in the flow which have a lifetime comparable to the biological time scales. Such structures are vortices in the flow, i.e. rotating

flow patterns, which are present in all ocean flows and which possess different sizes and life times. Since the average lifetime of vortices is of the order of days up to several weeks [13], such structures can be essential for the emergence of plankton blooms. The role of vortices as incubators of plankton blooms has been shown using different food web models in simple kinematic flows [14] as well as in turbulent flows [15]. The rationale behind this behavior is the fact that the water is mostly confined within the vortex due to the very low exchange with the surrounding waters. Therefore, plankton can grow without much disturbance within the eddy. Moreover, such coherent structures in flows may lead to a separation of different species having different needs of nutrients. This separation opens up ecological niches for different species to coexist and hence to a sustained biodiversity in the ocean [16].

To demonstrate this dynamics, we address now the question of coupling the biological model to a simplified hydrodynamic model, which mimics basic properties of ocean flows. More specifically we show the emergence of a harmful bloom in a von Karman vortex street which develops in the wake of an island. Though the underlying velocity field in a two-dimensional spatial region is given analytically [17, 18], the numerical procedure to obtain these patterns is slightly more complicated and therefore omitted here. We only present the result for a plankton model, which contains two different species, harmful and a non-harmful one competing for the same resource. This model is a bit more complex but relies on the same assumptions than the previous one (for details cf. [19]). The emergence of a harmful algal bloom in a vortex is illustrated in Fig.5. showing the abundances of the harmful species blooming mainly within the vortex. Such localized blooms can also be observed in satellite pictures of plankton blooms around the world (cf. http://oceancolor.gsfc.nasa.gov/cms/).

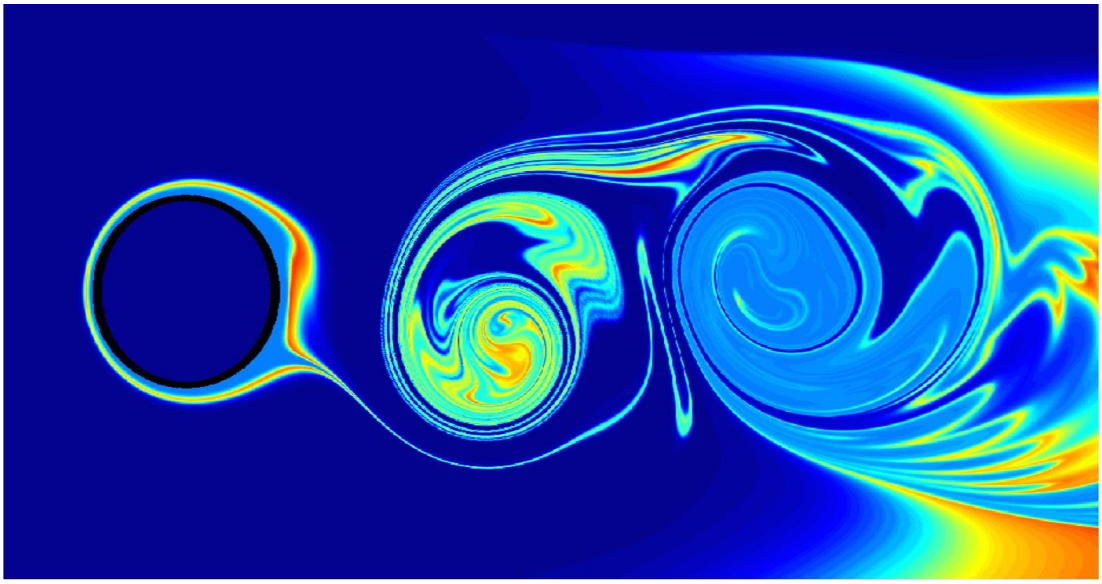

Fig.5. Phytoplankton bloom in a van Karman vortex street in the wake of an island: abundance is color-coded from blue for low abundance via green to orange for high abundance.

CONCLUSIONS

Interdisciplinary research on environmental problems requires an intimate interplay between different directions of science. To prepare high school students to those tasks and to get them acquainted to this much broader view on science it would be desirable if students would be exposed to questions, which are related to e.g. climate change. Utilization of such

simple approaches to ecological systems as demonstrated here could be one way to start educating students in a comprehensive view on the earth system.

ACKNOWLEDGMENTS

I would like to thank Tamás Tél and his group for their hospitality during my stay the Eötvös Loránd University Budapest and the Hungarian Academy of Sciences for their support.

REFERENCES

1. P. J. L. Williams, D. Thomas, C. S. Reynolds, *Phytoplankton Productivity*, Iowa State Press, Iowa City, 2002
2. D. M. Karl, E. A. Laws, Morris P. Williams P. J., Emerson S., Metabolic balance of the open sea, Nature, **426**, 32, 2003
3. U. Siegenthaler, J. L. Sarmiento, Atmospheric carbon dioxide and the ocean, Nature, **356**, 589, 1993
4. J. D. Murray, *Mathematical Biology I. Introduction*, Springer, Berlin, 1993
5. R. M. May, Simple mathematical models with very complicated dynamics, Nature, **261**, 459, 1976
6. C. S. Holling, Some characteristics of simple types of predation and parasitism. Can. Entomol., **91**, 385, 1959
7. L. H. Petterson, D. Pozdnyakov: *Monitoring of harmful algal blooms*. Springer, Berlin, 2013
8. D. M. Anderson, A. D. Cembella, G. M. Hallegraeff, Progress in understanding harmful algal blooms: paradigm shifts and new technologies for research, monitoring, and management. Annu. Rev. Mar. Sci., **4**, 143, 2012
9. P. J. S. Franks, Models of harmful algal blooms, Limnol. Oceanogr., **42**, 1273, 1997
10. D. J. McGillicuddy, Models of harmful algal blooms: conceptual, empirical, and numerical approaches, J. Mar. Syst. **83**, 105, 2010
11. J. E. Truscott, J. Brindley, Ocean plankton populations as excitable media, Bull. Math. Biol. **56**, 981, 1994
12. J. A. Freund, S. Mieruch, B. Scholze, K. Wiltshire, U. Feudel, Bloom dynamics in a seasonally forced phytoplankton-zooplankton model: Trigger mechanisms and timing effects, Ecological complexity, **3**, 129, 2006
13. D. B. Chelton, M. G. Schlax, R. M. Samelson, Global observations of nonlinear mesoscale eddies, Prog. Oceanogr., **91**, 167, 2011
14. M. Sandulescu, E. Hernandez-Garcia, C. Lopez, U. Feudel, Plankton blooms in vortices: the role of biological and hydrodynamic time scales, Nonlin. Processes Geophys. **14**, 1, 2007
15. A. Martin, Phytoplankton patchiness: the role of lateral stirring and mixing, Prog. Oceanogr., **57**, 125, 2003
16. I. Scheuring, G. Karoly, Z. Toroczkai, T. Tel, A. Pentek, Competing populations in flows with chaotic mixing. Theor. Popul. Biol. **63**, 77, 2003
17. C. Jung, T. Tel, E. Ziemniak, Application of scattering chaos to particle transport in a hydrodynamical flow, Chaos, **3**, 555, 1993
18. M. Sandulescu, E. Hernandez-Garcia, C. Lopez, U. Feudel, Kinematic studies of transport across an island wake, with application to the Canary islands, Tellus, **58A**, 605, 2006
19. D. Bastine, U. Feudel, Inhomogeneous dominance patterns of competing phytoplankton groups in the wake of an island, Nonlin. Processes Geophys., **17**, 715, 2010

MODELING CLIMATE CHANGE IN THE LABORATORY

M. Vincze
MTA-ELTE Theoretical Physics Research Group, Budapest, Hungary,
Brandenburg University of Technology, Cottbus-Senftenberg, Germany
mvincze@general.elte.hu

ABSTRACT

In a simple tabletop-size rotating wave tank experiment at the von Kármán Laboratory of ELTE, atmospheric climate change scenarios can be modeled by continuously decreasing the temperature difference between the two sidewalls of the tank, imitating the effect of global warming. As these boundary conditions slowly change, we can observe how the "weather" in the tank reacts to this non-stationary forcing. Such laboratory investigations may support the better understanding of the causal connections between global warming and the increasing number of unusually warm or cold seasons observed coincidentally in the past 30 years at the mid-latitudes of Earth.

INTRODUCTION

Understanding the underlying statistical properties of extreme weather conditions is crucially important to our society. Analogously to the engineering problem of sizing a dam to withstand extreme water levels, decision makers involved in long-term economic or political planning must consider and, if reasonably achievable, mitigate the risks of unlikely but highly hazardous events (e.g. to keep a certain amount of agricultural goods in reserve as preparation for extremely warm and dry Summers, as in the 3,500 year-old Biblical story of Joseph in Egypt). For such strategic purposes assigning odds to extreme events would be essential.

Unfortunately, quantifying such risks is far not trivial, firstly, because – by definition – extreme events are rare, thus reliable measurements are needed over as long time as possible. Even if this was granted, one must keep in mind that climate exhibits significant fluctuations on every imaginable timescale, yielding a power law-type long-range correlated behavior, as demonstrated by merging observational and paleoclimate data sets in, e.g. [1]. This feature implies that, strictly speaking, no data record can be long enough to define a stationary base period to which extremes can be properly compared. Yet, given the fact that only one realization of global temperature time series exists (we have one Earth, and we have no access to climate data from "parallel universes" with the same laws of physics but slightly different initial conditions), finding such "quasi-stationary" periods and taking them as the "golden standards" of climate variability is still the best thing climate scientists can do. It has some serious drawbacks, however, as we will point out.

Fig. 1 shows the monthly global average temperature anomalies of the Earth. By definition, anomalies are compared to the – relatively stagnant – three-decade base period of 1951-1980, whose temporal average is subtracted from the whole time series. As it is apparent from the graph, longer periods without any trend are more like the exceptions then the rule, as far as the past 150 years are considered.

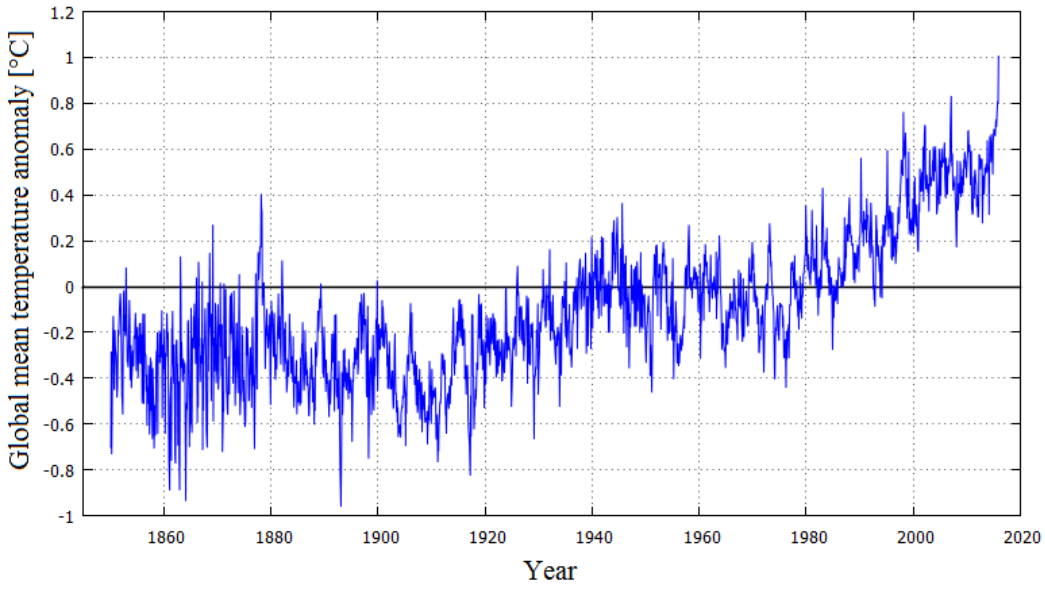

Fig.1. Fluctuations of monthly global mean temperature anomaly, as compared to the average of the 1951-1980 'base period'. Source: https://climexp.knmi.nl

Widely cited studies, such as [2] have come to the conclusion that coincidentally with the rapid global warming of the past 40 years, the so-called "climate dice", that describes the chance of unusually warm or cool seasons, has become more and more "loaded", or in other words, "the distribution of seasonal mean temperature anomalies has shifted toward higher temperatures and the range of anomalies has increased" (compared to their base period).

On the one hand, this is definitely a very interesting and important observation from the practical point of view; extremely hot summers can have disastrous effects on agriculture and our society in general. So this is clearly something important to know about, and prepare for. On the other hand, the finding, at least qualitatively, is exactly what one would expect from the simple fact that the time series of Fig. 1 in the considered period (i.e. the past 40 years) exhibits a marked increasing trend: if the mean is shifting upwards, previously rare high values more and more become the norm. The real question is therefore, whether the observed changes in the number of days in the year with "extreme temperatures" is merely a consequence of the shifting mean, while the statistical properties of the fluctuations (i.e. the physical nature of "weather") remain the same throughout the process, or there is also an inherent amplification within the dynamics of the fluctuations themselves, besides the shifting mean. Looking back to Fig. 1 the change in the past decades seems to be so rapid that even on the typical timescale of a larger fluctuation the trend line increases significantly: the observed process is nowhere near quasi-stationary. So the classic approaches of decomposing the signal to short term and long term components and identifying the former with "weather" and the latter with "climate forcing" can be very misleading.

The schematic drawings in the three panels of Fig. 2 are excerpts from the special report of the UN's Intergovernmental Panel on Climate Change (IPCC), titled "Managing the risks of extreme events and disasters to advance climate change adaptation" from 2012 [3]. Panel a) drafts the scenario of "shifted mean" in terms of the sketched probability density functions (PDFs) of global average temperature values. The graph corresponding to the base period is marked by solid line and the "climate change" scenario is sketched with the dashed curve. In this case the mean changes, but the fluctuations behave essentially the same way as in the base period. Panel b) shows just the opposite case: even though the mean does not change at all here ("no global warming" on the long term), yet, apparently something happens to the

weather system, because the "tails" of the PDF become thicker (i.e. frequencies of extremely hot or cold days in a year increase). Panel c) represents a similar scenario: the mean stays unchanged, and so does the "left tail" of the PDF, but the probability of hot weather increases, thus the symmetry of the distribution changes.

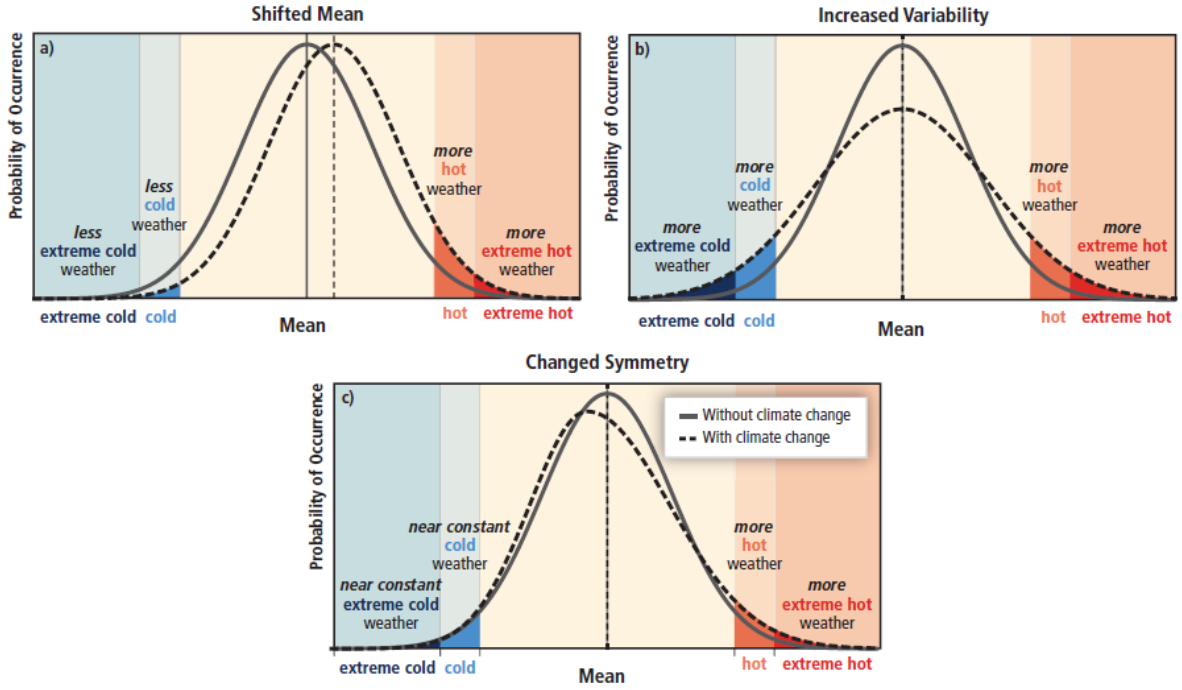

Fig.2. Sketches of probability density functions of the global mean temperatures subject to different "climate change" scenarios: a) shifting mean, b) increased variability, c) changed symmetry (source: [3])

The actual climate change probably cannot be described by any of these conceptual scenarios alone, but more likely as a combination of at least two of them. Yet, based on the available data, where – due to our incomplete understanding the climate system – separating the long-term deterministic components from stochastic fluctuations is practically impossible, therefore, it is hard to tell, which of the scenarios are actually contributing.

Since neither the true temporal behavior of the driving force (i.e. the climate system's response to changes in Solar flux, carbon-dioxide emission, etc.) nor the statistical properties of the fluctuations can be determined independently, the only proper way to take them apart would be to observe many realizations (paths) of the same dynamical system, presumably with very similar initial conditions and with exactly the same time-dependent forcing scenarios. Then statistical analyses over such an ensemble can be carried out and thus the separation of deterministic and stochastic terms (and the true properties of fluctuations around the mean) could be, at least theoretically, achieved.

Obviously, since only one realization of the actual climate system exists, ensemble statistics cannot be used there. However, there is a way to imitate climate-like dynamics in a surprisingly simple laboratory experiment. This, being a physical experiment, can be repeated and therefore ensemble statistics can be constructed, as will be discussed in the next sections. It is to be noted that this approach has been successfully applied to numerical climate models of minimal and intermediate complexity in very recent works, e.g. [4]. Surely, the outcomes from simplified laboratory experiments will not solve the problem of separating processes and obtaining proper extreme statistics from the actual global temperature records, yet, they may help to drive attention to some serious methodological issues which inevitably arise when using single-realization statistics instead of an ensemble.

EXPERIMENTAL SETUP AND METHODS

The so-called "differentially heated rotating annulus" is a widely studied experimental minimal model of the mid-latitude weather system. It is "minimal" in the sense that it captures the two most important basic factors that contribute to the formations of cyclones and anticyclones in the atmosphere: lateral temperature difference (between the polar and equatorial regions) and rotation (around the Earth's axis). If either of these boundary conditions was absent, no weather-like flow patterns would emerge; so the model is "as simple as possible but no simpler". For more details on the history and the possible variants of rotating annuli, we would suggest the reader to consult our recently published textbook chapter [5].

A schematic drawing and an actual photo of our experimental tank (alongside with a cartoon demonstrating the aforementioned analogy with the terrestrial atmosphere) is shown in Figs.3 b), c) and a), respectively. The annular gap between the coaxial cylindrical sidewalls is filled up with water to height d = 4.5 cm (Fig. 3b). The inner cylinder, with a separate working fluid in it, serves to maintain the desired "polar" temperature. It has a radius a = 4.5 cm, whereas the outer rim (where the warming occurs) is at distance b = 12 cm from the axis of rotation. The radial temperature difference ΔT yields an overturning "sideways convective" background flow, similar to the large convection cells in the actual atmosphere. Due to the rotation of the tank, Coriolis force also acts on the fluid parcels (that otherwise would trace out an azimuthally symmetric, toroidal overturning cell) and drags them towards the respective right hand side of their direction of motion (since, due to our 'Northern-hemisphere-chauvinism' counterclockwise rotation is applied here; Australian laboratories typically do it the other way, then the Coriolis force has an opposite sign). For more information on the Coriolis force, and the way it can be taught in high schools, we refer to the paper of Andrea *Gróf* in the present volume [6].

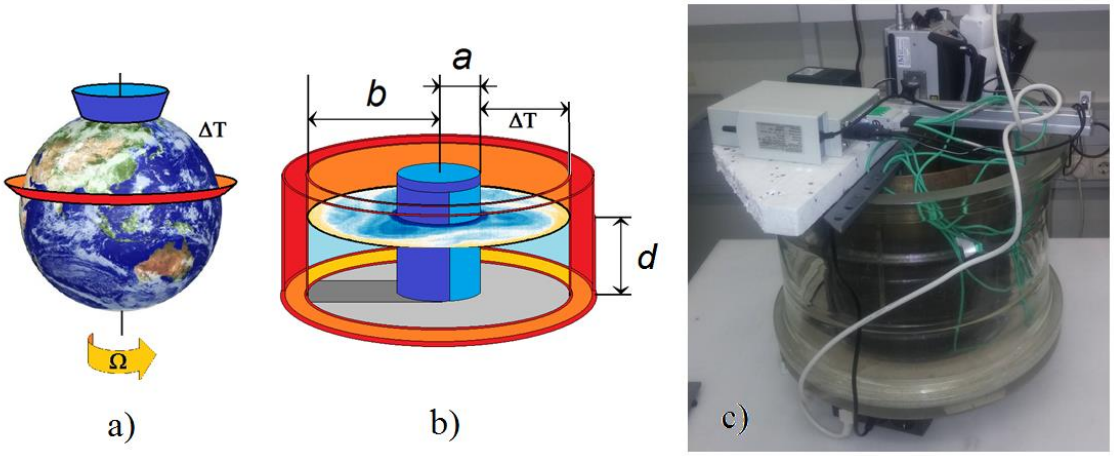

Fig.3. Schematic diagram of the mid-latitude atmosphere (a), illustrating that the basic boundary condition for it is a warm equator (red) and a polar region (blue) colder by temperature contrast ΔT. (b): Sketch of the differentially heated rotating annulus with its geometric parameters for which the boundary condition is similar to that of the real atmosphere: warm outer rim (red), cold inner rim (blue). (c): Photo of the actual experimental tank in the von Kármán lab

Coriolis force yields the formation of cyclonic and anticyclonic eddies, which can be seen by dye painting or via observing the water surface with a thermal (infrared) camera. A typical "atmosphere-like" flow pattern is visible in the left hand side of the composite image of Fig.4, alongside a satellite image of Earth as seen from poleward direction.

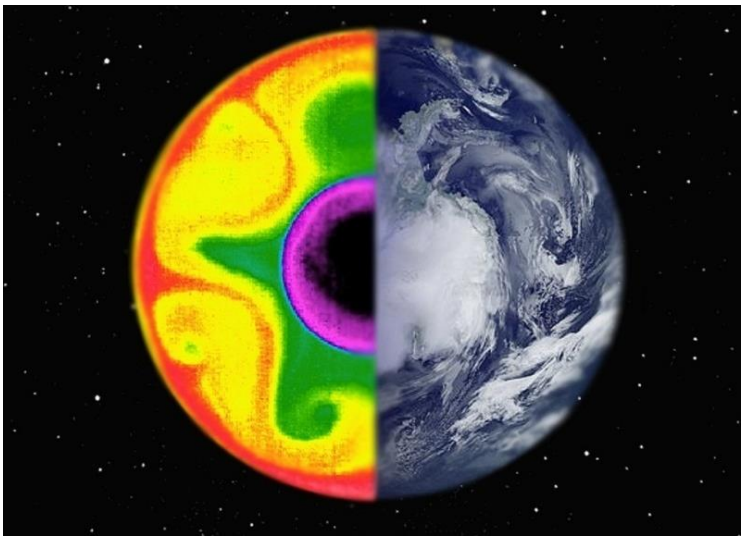

Fig.4. Infrared view of the flow in the laboratory setup (left) and cloud patterns of the Southern mid-latitudes as seen from space, looking down from the axial direction

The analogy between the atmosphere and the experimental configuration is of course far not qualitative only. Studying the equations of motion in both systems, one can derive two non-dimensional quantities that properly describe the possible flow regimes: these can be set in the experiment so that they match the same dimensionless ratios of the atmosphere. One of these parameter combination is known as thermal Rossby number *Ro*, and is defined as:

$$Ro = \frac{gd\alpha\Delta T}{\Omega^2(b-a)^2}, \tag{1}$$

where Ω is the angular velocity of the rotating tank, *a, b*, and *d* are the aforementioned geometric dimensions, α is the coefficient of volumetric thermal expansion of the fluid (water in the experiment and air in the atmosphere) and ΔT is the ("Equator-to-pole") temperature contrast imposed on the vertical boundaries of the rotating layer.

Besides *Ro* the kinematic viscosity *v* of the medium also plays an important role in the dynamics. Its contribution is parametrized by Taylor number *Ta* that accounts for the ratio of rotational and viscous effects, and reads as

$$Ta = \frac{4\Omega^2(b-a)^5}{\nu^2 d}. \tag{2}$$

Ro and *Ta* are used together to characterize the different dynamical regimes in rotating, thermally driven systems, such as planetary atmospheres, oceanic basins and their minimal models in the laboratory. The parameter space with a few typical snapshots of the corresponding experiments is sketched in Fig.5: for smaller rotation rates, where the Coriolis force is of less importance (green shaded area) the flow stays axially symmetric. In an intermediate "anvil-shaped" domain of moderate *Ta* and smaller *Ro* values regular three- or four-fold symmetric wave structures emerge (orange domain), and towards higher rotation rates (larger *Ta* and small *Ro*) the flow becomes turbulent. The letter is the domain where Earth's mid-latitude atmosphere also belongs, once its actual physical parameters are plugged in the above formulae of *Ta* and *Ro*.

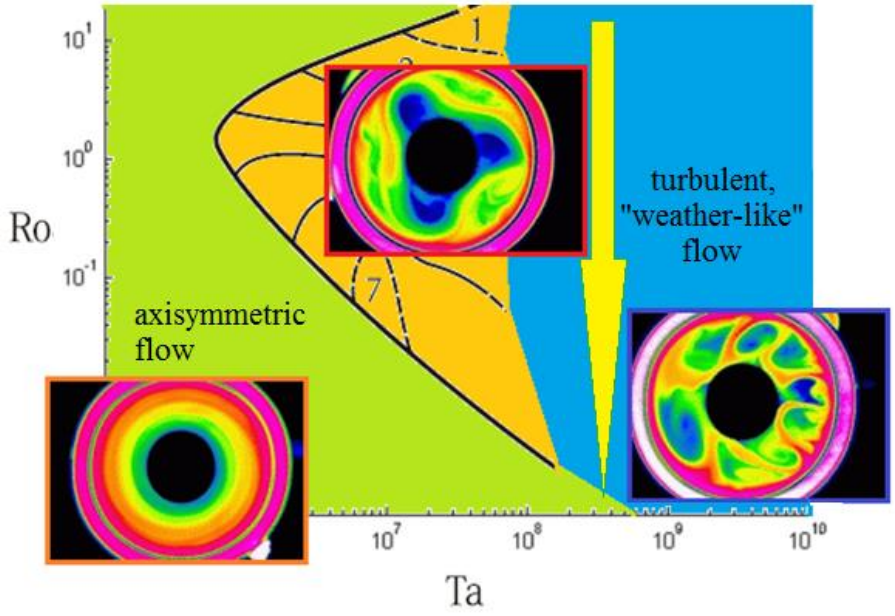

Fig.5. Regimes of the *Ta*-*Ro* parameter space with the observed flow patterns (insets). The yellow arrow shows the shift due to decreasing radial temperature contrast

The novelty of our experiments [7] carried out in the von Kármán lab and at the Brandenburg Technical University of Cottbus (Germany) is the following procedure: while keeping the rotation rate, thus, Taylor number *Ta*, constant – so that a "day" i.e. a full revolution of the tank lasted for 3 seconds – after a true "base period" of ca. 3000 revolutions of constant ΔT, we started to decrease the temperature contrast parameter, by turning off the computer-controlled cooling of the "polar" thermostat. After this change of the thermal boundary conditions we logged the data for another 3000 revolutions of time, corresponding to a "global warming" scenario with gradually increasing polar temperatures.

It is a well-established fact that the ongoing global warming of the Earth affects the polar regions the most in terms of mean temperature (melting sea ice and land ice), whereas in the local records from the equatorial regions the warming trend is not that apparent. Thus, climate change yields gradually *decreasing* mean equator-to-pole temperature contrast; this is what we imitated in the lab by lowering ΔT. Such a "global warming" in our experiment corresponds to a downward motion in the parameter space of the system, marked by a yellow arrow in Fig.5.

We repeated the very same forcing scenario 10 times with the same initial conditions, in order to create a statistical ensemble of virtually identical experimental runs, which only differed in the stochastic aspects of their evolution. We logged mean surface temperature $\langle T \rangle(t)$, defined as the spatial average of temperature signals obtained simultaneously from three digital thermometers placed on the water surface inside the annular gap of the tank. Their sampling rate was 1 Hz, and their temperature resolution was below 0.05 K.

PRELIMINARY RESULTS

Fig. 6 shows time series obtained for four typical experimental runs. In the top panel, the imposed temperature contrast forcing scenarios $\Delta T(t)$ are plotted, as obtained from the differences of measured temperatures at the heated and cooled lateral sidewalls. One can see that the reproduction of the experiments is very good. In each case, time $t = 0$ corresponds to the time instant when the cooling thermostat was switched off. The bottom panel shows the 'response' of the mean surface temperature $\langle T \rangle(t)$ in each run (colored curves) and their

ensemble average (thick black curve). As expected, the latter is much smoother than any of the realizations: the stochastic fluctuations of the different runs average out fairly enough. Note also, that the response ensemble average does not exhibit a sharp turning point at $t = 0$; the transition towards "global warming" appears to be a continuous one, even in terms of its derivative, unlike the forcing itself.

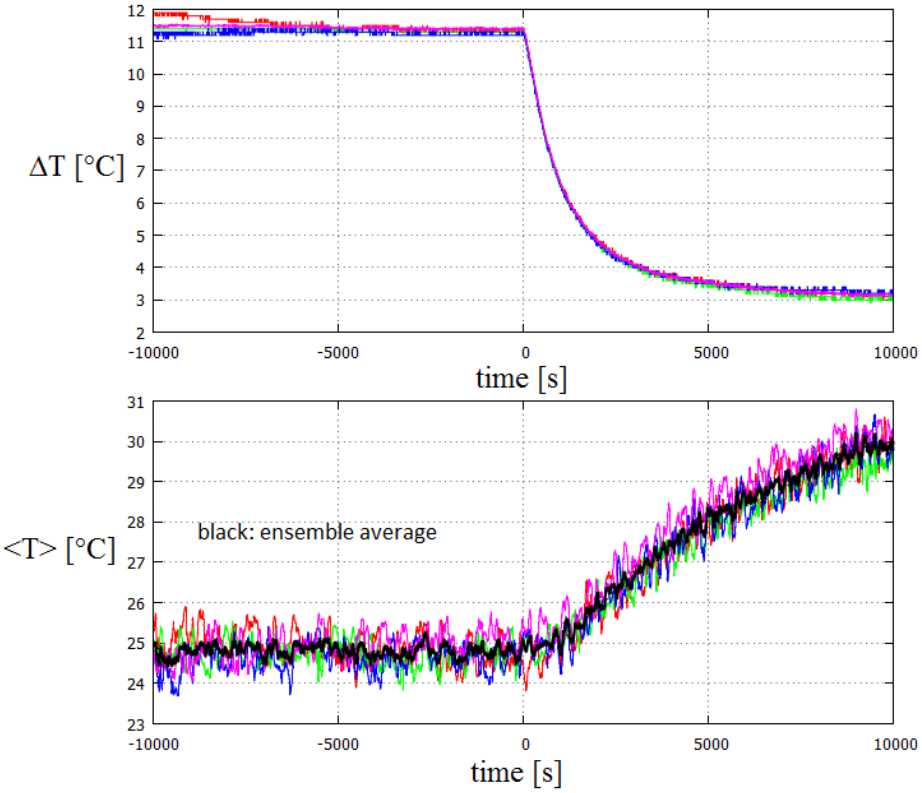

Fig.6. Time-dependence of temperature contrast $\Delta T(t)$ in four experimental runs (top) and the resulting records of "global warming" $\langle T\rangle(t)$ from the same experiments (bottom). The ensemble average is marked with black curve (data from our experiments at BTU-Cottbus)

To demonstrate our main point here, let us consider one of the realizations – namely, the red curve of Fig. 6, repeated in Fig. 7 – and treat it the same way as climate scientists analyse actual atmospheric data. Pretending that we do not have any *a priori* knowledge of the underlying forcing scenario, the best we can do to analyse fluctuations is to apply polynomial de-trending of the temperature record. This is achieved by fitting a polynomial function to the time series $\langle T\rangle(t)$ and subtract it from the original record afterwards. Two such polynomial fits are shown in the top panel of Fig. 7: a sixth-degree (green) and a tenth-degree one (blue). The ensemble average is repeatedly plotted here, too (black curve).

In the next step – as a measure of variance – we calculated the 1001-point, or 300 revolution-long (centered) moving standard deviations of $\langle T\rangle(t)$ defined as

$$\sigma_{1001}^{(i)} = \sqrt{\frac{1}{1001}\sum_{i-500}^{i+500}\left(\langle T\rangle^{(i)} - m_{1001}^{(i)}\right)^2}, \qquad (3)$$

where index i is running from the 501th measured value of time series $\langle T\rangle(t)$, up to $i = N - 501$, N being the total number of data points in the record. $m_{1001}^{(i)}$ is the moving mean in the same window, obtained as

$$m_{1001}^{(i)} = \sum_{i-500}^{i+500}\frac{\langle T\rangle^{(i)}}{1001}. \qquad (4)$$

The moving standard deviations of the original time series $\langle T \rangle(t)$ are shown with red in the bottom panel of Fig. 7. This can be understood as an estimated measure of "atmospheric variability": the larger its value, the more the time series fluctuates around the running mean. This is no surprise that here, without detrending, the variability increases instantly from around $t = 0$ on due to the increasing trend.

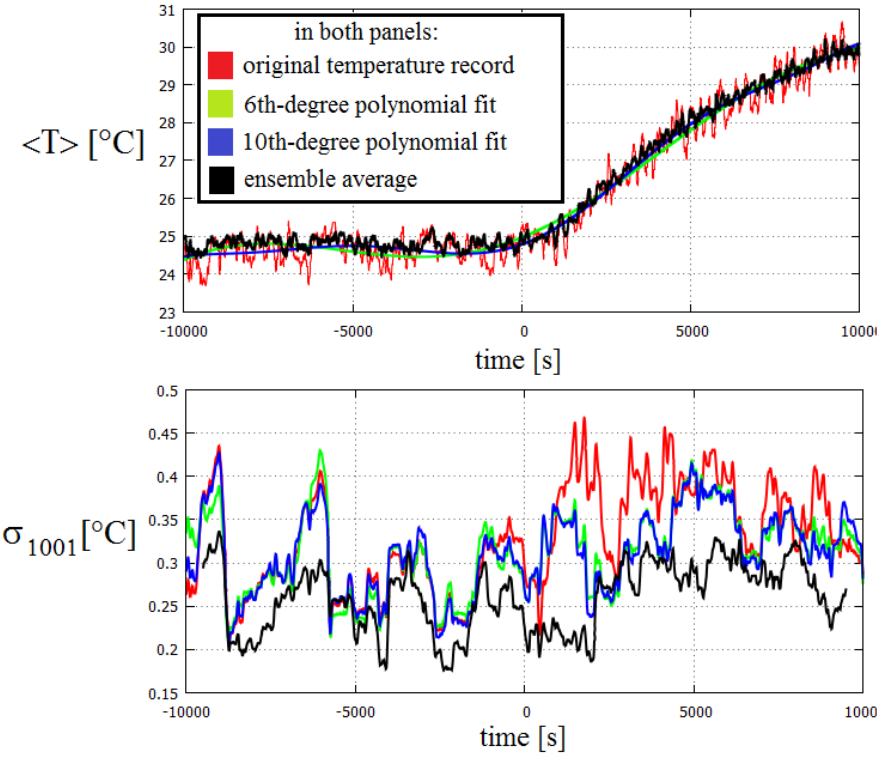

Fig.7. Top: A single realization of the mean surface temperature $\langle T \rangle$ (red), its polynomial fits (green and blue) and the ensemble average (black). Bottom: standard deviations of the original record (red), those of the detrended records (green and blue), and those obtained after subtracting the ensemble average from the temperature record (data from our experiments at BTU-Cottbus)

Afterwards, we carried out the same procedure with the *detrended* records as well: the moving standard deviations and moving averages were calculated in the same manner as written in formulae (3) and (4), but instead of the original $\langle T \rangle(t)$ now the detrended time series were evaluated. The results are plotted in the bottom panel of Fig. 7: the green and blue curves represent the moving standard deviations of the sixth and tenth-degree detrended records, respectively. We found in both cases that the average variabilities are significantly higher in the $t > 0$ range than before, although clearly, immediately after $t = 0$ these detrended records yield smaller fluctuations than the values of the red curve. Therefore, if these were real global temperature data and this would be the only known realization, a climate scientist would come to the conclusion that the internal variability of the system indeed increased coincidentally with the warming, as compared to the stationary base period ($t < 0$).

However, if we use the ensemble average (shown as black curve in the bottom panel of Fig. 6 and in the top panel of Fig. 7) for detrending, i.e. subtract its values from the original $\langle T \rangle(t)$ and calculate the moving standard deviations of the obtained detrended time series (black curve in the bottom panel of Fig. 7), we get a different result. Apparently, these variabilities appear to be systematically below and more uniform than, both polynomial residuals. In other words, fluctuations of the mean temperature around the ensemble average

are *smaller* than even around the record's own polynomial trend. The other important observation is that unlike in the cases of polynomials, detrending with the ensemble average does not yield significant difference between the mean fluctuations in the base period ($t < 0$) and the "global warming" phase ($t > 0$), demonstrating that even high-degree detrending – based on the considered realization only – can produce "artificial" changes in the variability.

SUMMARY AND CONCLUSIONS

Experiments in the von Kármán Laboratory offer a unique insight into the large-scale dynamics of flows in the atmosphere and the ocean. In the present work the behavior of atmospheric variability in a changing climate has been studied in an experimental 'toy model' of mid-latitude atmosphere. Unlike in the case of real climate, in laboratory experiments it is possible to run the same scenario several times, thus creating a statistical ensemble. A large enough data pool enables the separation of the deterministic and stochastic aspects of temperature variations in the system. This was demonstrated by using standard tools of time series analysis on temperature records of several identical experiments. We concluded that if the fluctuations of an individual realization are compared to the proper (constantly shifting) ensemble average, no significant changes occur in their variability, as compared to a stationary base period.

These results have a certain methodological or demonstrational value and may help to increase awareness in the climate community of the fact that – as long as the underlying complex processes are not properly understood *a priori* – fluctuations and deterministic trends can hardly be separated, and therefore they may well yield statistical artifacts that can easily be misinterpreted.

ACKNOWLEDGMENTS

The present work was supported by EuHIT (European High Performance Infrastructures in Turbulence) and by OTKA grant, no.: NK100296. Highly useful discussions with Tamás Tél are very much acknowledged.

REFERENCES

1. P. Huybers, W. Curry: Links between annual, Milankovitch, and continuum temperature
   variability, Nature, **441**, 329, 2006
2. J. Hansen, M. Sato, R. Ruedy: Perception of climate change, Proceedings of the National Academy of Sciences, **109**, E2415, 2012
3. C. B. Field et al. (eds.): Managing the risks of extreme events and disasters to advance climate change adaptation – Special report of the Intergovernmental Panel on Climate Change, Cambridge University Press, Cambridge, 2012
4. G. Drótos, T. Bódai, T. Tél: Probabilistic Concepts in a Changing Climate: A Snapshot Attractor Picture, Journal of Climate, **28**, 3275–3288, 2015
5. M. Vincze, I. M. Jánosi: Laboratory experiments on large-scale geophysical flows, in: *The Fluid Dynamics of Climate (CISM Courses and Lectures, Vol. 564.)*, eds: A. Provenzale, E. Palazzi, and K. Fraedrich, Springer, Vienna, CISM Udine, pp 61-94, 2016
6. A. Gróf: Carousels to Coriolis, or how physics supports understanding geography, present volume
7. M. Vincze, U. Harlander: Temperature fluctuations in a changing climate: an ensemble-based experimental approach, submitted

APPENDIX: THE VON KÁRMÁN LAB

The von Kármán Laboratory for Environmental Flows of the Institute of Physics at the Eötvös University (ELTE) of Budapest is one of the very few of its kind in Europe. Based on the principles of hydrodynamic similarity, large-scale atmospheric and oceanic phenomena (shallow-water waves, tsunamis, weather fronts, atmospheric convection, cyclones, tornados, etc.) can be accurately modelled and demonstrated here in relatively simple, table-top-size experimental setups [1].

Our laboratory was founded in 1998, when a group of enthusiastic physicists, namely V. *Horváth*, I. M. *Jánosi*, G. K. *Szabó*, and T. *Tél* – by then already internationally recognized experts in their own fields, ranging from chaotic dynamics to materials science – developed an interest in the surprisingly nontrivial and modern field of geophysical fluid dynamics. ('Modern' is meant in the sense that the proper theoretical framework of atmospheric dynamics was mainly developed after the 1920s, and even later for oceanic flows. Thus, being a contemporary of quantum mechanics, it can indeed be rightfully regarded as 'modern classical physics'.)

The then-newly constructed campus and the relocation of the Institute of Physics to it from its previous historic building (where even Eötvös himself used to work around the turn of the last century), provided a very fortunate once-in-a-lifetime opportunity to obtain two rooms and financial support for creating such a laboratory in the new building. In the almost 18 years since then, von Kármán lab has matured indeed, and evolved into a superb educational and demonstrational hub, where – as a part of their standard curriculum – bachelor and master students in physics, meteorology or environmental science regularly attend classes, participate in laboratory practices, and some of them eventually end up doing their thesis work here.

Besides education, however, the lab, first and foremost, is a research institution. Even during a regular laboratory practice here, students often face problems for which the solution is simply not known yet. They help us collecting data points for active research projects and in turn, they get a glimpse into how science works, where pretty often even the teacher or laboratory assistant cannot predict the outcome of a given experiment either. Several research topics that started here as bachelor's or master's projects later have actually evolved into publications in peer-reviewed international scientific journals. Three PhD degrees have been earned in our lab (one by the author) so far, and currently our regular staff consists of two senior researchers, one post-doc, a PhD student, and a BSc student. As of today, we are running five different environmentally motivated research projects (three of which are collaborative efforts, involving international partners), see the collage of snapshots in Fig.8, one of which has been discussed in the present work.

It is fair to say that the results coming from the von Kármán lab are of comparable quality to those from any environmental fluid dynamics laboratory in the world; similar research facilities are located at the Universities of Oxford, Cambridge (UK), Aix-Marseille (France), the Brandenburg Technical University at Cottbus (Germany), and at MIT (USA).

The laboratory is open for high school groups to visit at any previously agreed-upon time (preferably Fridays): a typical 'lab tour' lasts for ca. 40 minutes and an ideal group consists of up to 12 students. As Fig.9. shows there is practically no lower limit for the age when a lab tour can be interesting for the children: here a group of kindergarten kids are apparently mesmerized by a demonstration of internal waves in a stratified fluid tank. We can say it with confidence that these experiments can be interesting for toddlers and university professors alike.

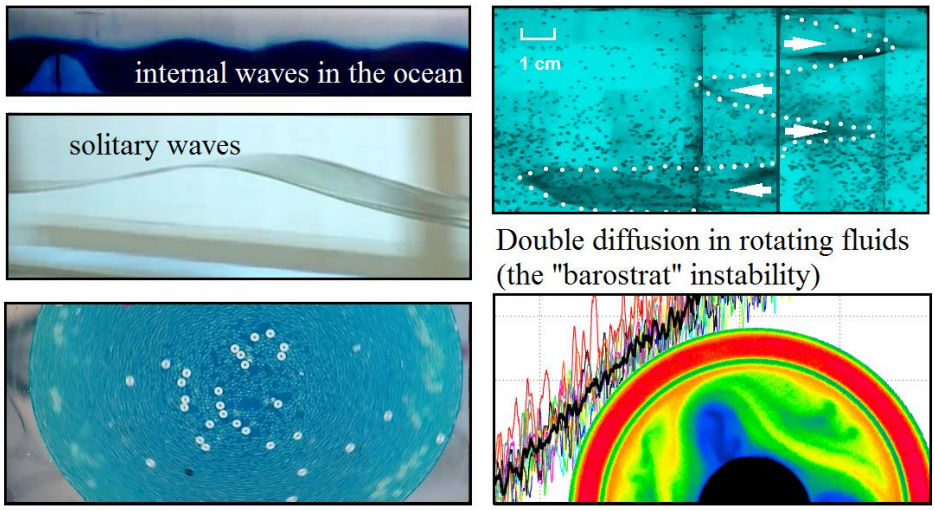

Fig.8. Snapshots from some of the currently active research areas in the von Kármán laboratory

Fig.9. "Visiting researchers" from a kindergarten (and the author) observe internal wave propagation in the von Kármán lab (2015)

Finally, it is appropriate to mention here that – to our great pleasure – the von Kármán lab is not any more the 'only place in its 800-kilometer radius where large-scale environmental flows can be demonstrated experimentally', as we used to claim. We refer to the paper of A. *Vörös* in the present volume [2], which describes somewhat similar experiments for educational purposes at the Babes-Bolyai University of Cluj-Napoca, Romania, and their usage to demonstrate tsunamis, weather fronts and cyclones for high school pupils.

REFERENCES

1. http://karman3.elte.hu/index_eng.php
2. A.Vörös, Zs. Sárközi: Promoting environmental physics issues in science centers and at science-events, present volume

CAROUSELS TO CORIOLIS, OR HOW PHYSICS SUPPORTS UNDERSTANDING GEOGRAPHY

Andrea Gróf
Karinthy Frigyes Gimnázium, Budapest, Hungary, gandi@karinthy.hu
Physics Education PhD Program, Eötvös University, Budapest

ABSTRACT

There is a conflict between the ways motions are described in physics and geography classes. While non-inertial frames do not feature in official physics curricula, geography texts rely on inertial forces in explaining motions of the atmosphere and the seas. Prompted by a survey demonstrating that the physical principles behind geography are not understood, this paper presents a possible treatment within the limits of high-school mathematics. Through the classic example of a merry-go-round, inertial forces are introduced quantitatively, and the results are applied in problems related to motions in geography.

INTRODUCTION

The choice of reference frame is a central idea in the physics class, while in geography they just use their "natural" frame without addressing the issue of reference frame at all. Furthermore, that frame is a non-inertial one, whereas we at most switch from one inertial frame to another, and may even reproach our students if they dare to say "centrifugal force". When geography is taught in year 9, underlying physical concepts and principles are either lacking, or recently acquired knowledge is not yet supported by sufficient experience. Explanations given by geography texts are often superficial or even wrong, but the conflict exists even in the case of a correct approach. With more background knowledge and expertise in problem solving, it is worth revisiting geographic phenomena in physics lessons later on.

A SURVEY ON PHYSICS BEHIND GEOGRAPHY

A multiple choice survey with 215 students revealed a serious lack of understanding, with no significant difference regarding whether they had completed geography before physics, or they had studied both subjects in the same year. The survey encompassed a wide range of concepts related to timekeeping, the shape of the Earth, motions of air and the seas, etc. Two of the questions involving inertial forces are shown below.

One question tested the understanding of the nature of such forces: "The oblate shape of the rotating Earth is generally explained in terms of the centrifugal force. On the other hand, in physics problems dealing with circular motion and rotation, no centrifugal forces were considered. What is the difference?" The correct answer of different frames was only chosen by 17%. Distractor answers (based on classroom experience, and possible misinterpretations of geography texts) would deserve deeper analysis but that is beyond the scope of this paper.

Another question addressed the perennial myth of the kitchen sink: "Ivan in Moscow and Pedro in Buenos Aires each fill the kitchen sink with water and remove the stopper. The water drains with a whirl. What will they observe?" Only 10% gave the correct answer. The most popular distractor (56%) was the one stating that water whirls counter-clockwise for Ivan and clockwise for Pedro. This suggests that students learn their geography regarding cyclones, and apply it without criticism to anything that rotates. Just like Sylvester Stallone in Escape Plan, observing the toilet and concluding that the prison is on the southern hemisphere.

The myth is reinforced by "demonstrations" of the Coriolis force performed to tourists at the Equator, showing how draining water whirls one way or the other if the apparatus is moved a few metres to the north or to the south. They all cheat since the horizontal Coriolis force is zero at the Equator and varies as the sine of the angle of latitude. See [1] for an amateur video to observe angular momentum created by pouring water in a sink from the appropriate side. Tourists give credit to the presentation, although deception is quite apparent. It is instructive to reproduce the "demonstration" in class. (Just draw a random line on the floor and call it the Equator.)

INTRODUCING INERTIAL FORCES

The merry-go-round is a standard illustration of a rotating reference frame. However, high-school level resources normally offer conceptual treatment only. The approach demonstrated here is quantitative, without resorting to any vector calculus or even a vectorial product. Since it applies a lot of the dynamics taught in the regular curriculum, it can be used as a kind of synthesis, adding a little extra at the end of the year.

The programme features a rotating observer A whose reference frame is attached to the centre and rotates along with the roundabout, an inertial observer B, and two further characters: a lizard running along the rim, and a sparrow scared away and flying radially (Fig. 1). Numerical values are calculated in each case, to give an idea of how various forces or accelerations compare to each other.

Suppose the mass of A is 20 kg, the radius of the carousel is 1.5 m, and it completes a revolution in 3 s. As seen by B, the speed of A is then v = 3.14 m/s, and she is acted on by a net force of $m\omega^2 r$ = 132 N. It is important for students to understand that this is the inward push by the merry-go-round seat, and since it is a real force exerted by a real object, the same force must be present in A's frame, too. Since A is in equilibrium in A's frame, that raises the need for an extra outward force of magnitude $m\omega^2 r$, so the centrifugal force is introduced.

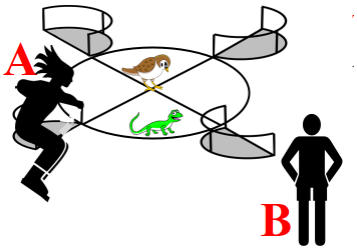

Fig.1. The four characters

Next, the motion of the lizard is considered in each frame. Assume its mass is 20 g and it runs at a speed of u = 0.50 m/s along the rim. Again, the observers must agree on the force exerted by the merry-go-round. That constitutes the net force for observer B (Fig. 2, top left):

$$F_{\text{net}} = F_{\text{merry}} = ma = m\frac{(v+u)^2}{r} = 0.0200 \cdot \frac{3.64^2}{1.50} = 0.177\text{N}\,. \qquad (1)$$

For rotating observer A, however, the speed of circular motion is only 0.50 m/s, and the net force is only 0.003N, so outward forces need to be added to the merry-go-round force of 0.177 N to produce a resultant of 0.003N. One such force is the centrifugal force of $m\omega^2 r$ that is calculated to be 0.132 N, but that alone will not produce the required resultant. Yet another outward force of $-0.003+0.177-0.132=0.042\,\text{N}$ is needed. What is the physical law behind that? Let us examine the forces and accelerations algebraically. Expand the square in (1):

$$F_{\text{merry}} = m\frac{(v+u)^2}{r} = \frac{mv^2}{r} + \frac{2mvu}{r} + \frac{mu^2}{r}\,. \qquad (2)$$

The last term of (2) represents the net force for A, a resultant of real and inertial forces:

$$\frac{mu^2}{r} = F_{\text{merry}} - \frac{mv^2}{r} - \frac{2mvu}{r}\,. \qquad (3)$$

The first term of (3) is the inward real force of the seat, the second term is the centrifugal force outwards, and the last term is the missing force, also outwards this time. Thus an object moving tangentially at speed u is acted on by a force $2mvu/r = mu \cdot 2\omega$. This is the Coriolis force, and substitution of numerical data yields the magnitude of 0.42 N.

Figure 2 below summarizes the forces in the two frames. The direction of the Coriolis force is the opposite when the lizard is running the other way. A special case of this situation occurs when A observes the motion of B, who stands on the ground, a distance R from the centre. According to A, he is moving in a circle at a tangential speed of $u = -\omega R$, that is, his (net) acceleration is $a = \omega^2 R$. Since there is no real horizontal force exerted by other objects on him, this acceleration is caused by the two kinds of inertial forces: the outward centrifugal acceleration $\omega^2 R$, and an inward Coriolis acceleration of $2\omega u = 2\omega^2 R$. So the resultant is $a = 2\omega^2 R - \omega^2 R = \omega^2 R$ inwards.

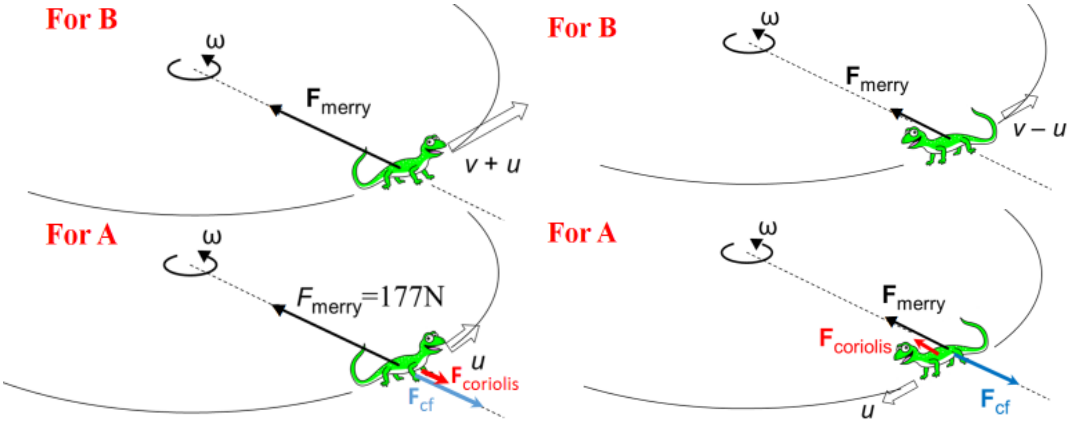

Fig.2. Forces on an object moving tangentially.
Left panel: in the direction of rotation, Right panel: opposite to the direction of rotation

So far, we have investigated objects in tangential motion and radial forces acting on them. The motion of the sparrow flying away from the centre is uniform and radial for B, but rather complex from the point of view of A. Radial acceleration is zero in A's frame, too, (like for the motion of B in the previous example,) but the tangential speed is increasing in proportion to the distance, so this time there is a tangential force, too. Figure 3 (right panel) shows the constant radial speed and increasing tangential speed of the sparrow at equal intervals of Δt.

If the distance from the centre increases by Δr in a time Δt, then $v = \Delta r/\Delta t$. In a short time Δt, acceleration can be considered uniform, angular displacement increases by $\omega\Delta t$, which means a distance of $\omega\Delta t \cdot \Delta r$ covered in a direction perpendicular to the radius. That is,

$$\frac{1}{2} a(\Delta t)^2 = \omega\Delta t \cdot \Delta r \,.$$

$$a = \frac{\Delta r}{\Delta t} \cdot 2\omega = v \cdot 2\omega \,.$$

The same formula is found to apply to the sideways force due to radial motion as to the sideways force due to tangential motion. Hence, it applies to every motion in a plane perpendicular to the rotation axis. The treatment of the Coriolis force is completed.

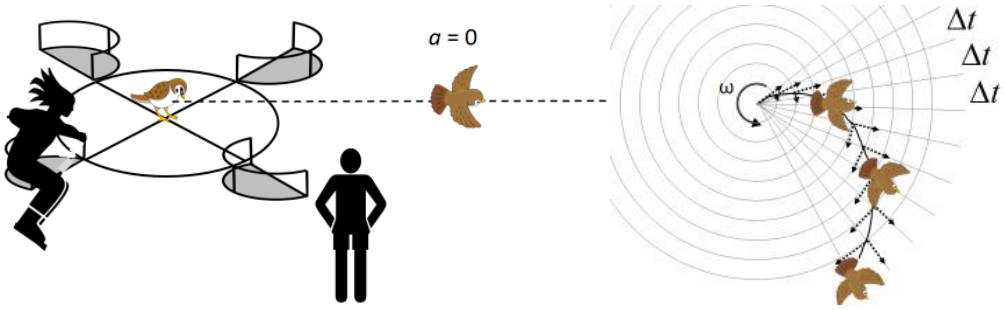

Fig.3. The motion of the sparrow as it appears to B (left panel) and A (right panel)

APPLICATIONS ON THE ROTATING EARTH

The selection below gives some outlined and some worked examples of quantitative exercises related to geography. Note that the angular speed of the Earth is $\Omega = 7.292 \cdot 10^{-5}$/s.

Exercise 1. Free fall acceleration is the resultant of gravitational acceleration towards the centre and centrifugal acceleration away from the axis. Thus, g is found to be 9.78 ms^{-2} at the Equator. The value of g influences sports results: for example, if an athlete can jump 8.00 metres at the poles then, assuming the same initial speed and angle, his jump is calculated to be 4.04 m at at the Equator.

Exercise 2. Budapest lies at a latitude of N47.5°. Find the magnitude and direction of the centrifugal acceleration and of the free fall acceleration at Budapest. Calculate with the average radius of the Earth, R = 6370 km.

Solution. $a_{cf} = \Omega^2 \cdot R\cos\varphi = (7.29 \cdot 10^{-5})^2 \cdot 6.37 \cdot 10^6 \cdot \cos 47.5° = 0.023 \frac{\mathrm{m}}{\mathrm{s}^2}$,

directed away from the axis of rotation. The magnitude of the vector sum (Fig. 4) with the gravitational acceleration towards the centre is obtained by using rectangular components:

$$a_g = \gamma \frac{M}{R^2} = 6.672 \cdot 10^{-11} \cdot \frac{5.974 \cdot 10^{24}}{(6.370 \cdot 10^6)^2} = 9.823 \frac{\mathrm{m}}{\mathrm{s}^2}.$$

$$g = \sqrt{(9.823 \cdot \cos 47.5° - 0.023)^2 + (9.823 \cdot \sin 47.5°)^2} = 9.81 \frac{\mathrm{m}}{\mathrm{s}^2}.$$

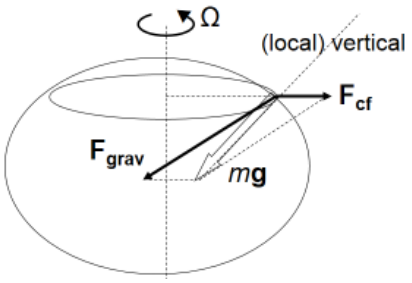

Fig.4. The direction of free fall acceleration

Its direction is somewhat to the south of towards the centre. This is what "down" means; the flattened shape of the Earth formed to make the surface perpendicular to this direction.

Exercise 3. To link with the merry-go-round example, the Coriolis force should first be investigated at the Equator. Suppose wind is blowing at a speed of u = 20 m/s towards the west at the Equator. The Coriolis acceleration is found to be $2\Omega u = 2.9 \cdot 10^{-3}$ ms^{-2}, directed vertically downwards. Note that its direction is radial, that is why the whirling water "demonstrations" are hoaxes.

Exercise 4. At other latitudes the Coriolis force has a horizontal component, too. Since we consider motions in a plane perpendicular to the local vertical rather than to the axis, the situation is more complex than the carousel case. High-school texts normally refer qualitatively to Foucault's pendulum as demonstration, but they do not explain the value of the local angular speed. By a high-school level adaptation of the explanation (based on the transport of vectors on curved surfaces) offered by some advanced texts (e.g. [2]), the use of angular velocity vector and components may be avoided: Students know that the surface of a cone unfolds in a plane. Consider the cone touching the globe along the φ = N48.8° parallel of Paris (Figure 5). In one day, while the Earth turns through 2π, Paris (point P) only turns in the unfolded plane by an angle of $2\pi\cdot\sin\varphi$. Hence the local angular speed is $\sin\varphi$ times that of the Earth:

$$\omega = \Omega\cdot\sin\varphi = 7.29\cdot10^{-5}\cdot\sin48.8° = 5.49\cdot10^{-5}\,/\,\mathrm{s}$$

which means 11.3° per hour. It would be 15° at the poles and zero at the Equator.

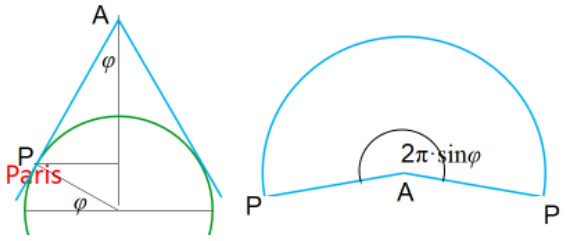

Fig.5. Demonstration of turning in a plane perpendicular to the local vertical

Exercise 5. (a) The mystery of the kitchen sink unravelled at last. Calculate the acceleration of a bread crumb in Budapest, circling at a radius of 2 cm, at a speed of 10 cm/s. What part of the acceleration is due to the Coriolis force? (b) Answer the same question for Jupiter's great red spot, a giant whirlwind at S22° latitude, angular size 25° by 12°. Wind speed is in the order of 100 m/s. The radius of Jupiter is about 72 000 km, and it rotates fast, completing a revolution in 9.8 hours. (Based on [3].)

Solution. (a) $$a = \frac{v^2}{r} = \frac{0.1^2}{0.02} = 0.5\,\mathrm{m/s^2}.$$

$$a_C = 2v\Omega\sin\varphi = 2\cdot0.1\cdot(7.3\cdot10^{-5})\sin47.5° = 1\cdot10^{-5}\mathrm{m/s^2}.$$

The effect is very small compared to other effects responsible for the motion, such as the geometry of the sink or the initial angular momentum that the water happens to have.

(b) 1° on Jupiter corresponds to $2R\pi/360 = 1.2\cdot10^6$ m, so the roughly 9° radius of the spot means an acceleration of about $9\cdot10^{-4}$ ms^{-2}, while the Coriolis acceleration is found to be about $1\cdot10^{-4}$ ms^{-2}. It is comparable to the net acceleration, so the Coriolis force does play a role in the formation of this persisting storm.

Exercise 6. (a) A golfer in Scotland, N55° latitude, can hit the ball to 300 m at a 45° angle. (b) An artillery missile is launched at 700 m/s. Does the deviation owing to the Coriolis force need to be considered? (Calculate the sideways deflection owing to the Coriolis force.)

Solution. (a) Using the known formulae of projectile flight, a range of 300 m implies an initial speed of 54 m/s, and a flight time of 8.7 s. Hence

$$d = a_C\frac{t^2}{2} = (2\cdot\Omega\sin\varphi\cdot v_0\cos\alpha)\frac{t^2}{2} = 7.3\cdot10^{-5}\cdot\sin55°\cdot54\cos45°\cdot8.7^2 = 17\,\mathrm{cm}.$$

The deflection is probably negligible compared to other disturbing effects like wind.

(b) The range is now 50 km, and the sideways deflection is about 300 m. This time, the effect is significant, it has to be considered in aiming the missile.

Exercise 7. What happens if a hockey puck is hit in a perfectly frictionless ice rink? Not straight line motion! The net force on the puck is not zero in the rotating reference frame of the Earth. If the ice is perfectly horizontal, that is, perpendicular to the local vertical, all other forces will cancel, leaving the horizontal Coriolis force, a sideways force as resultant. That leads to circular motion.

Exercise 8. How fast should we hit the puck in Budapest so that the circle fits in an ice rink 30 m wide? (Based on [3].)

Solution.

$$a_{\text{centripetal}} = \frac{v^2}{r} = 2\Omega \sin\varphi \cdot v \quad .$$

$$v = 2\Omega \sin\varphi \cdot r = 2 \cdot 7.3 \cdot 10^{-5} \cdot \sin 47.5° \cdot 15 = 0.61 \frac{\text{mm}}{\text{s}} \quad .$$

Quite slow. For speeds in the order of a metre per second, we need r = 9.3 km in Budapest (39 km at 10°, and 7.0 km at 80° latitude). Such large ice rinks we do not have, but nature realizes this kind of motion. Figure7 below shows the positions of a buoy in the Baltic sea, southeast of Stockholm at N57° latitude [4],[5].

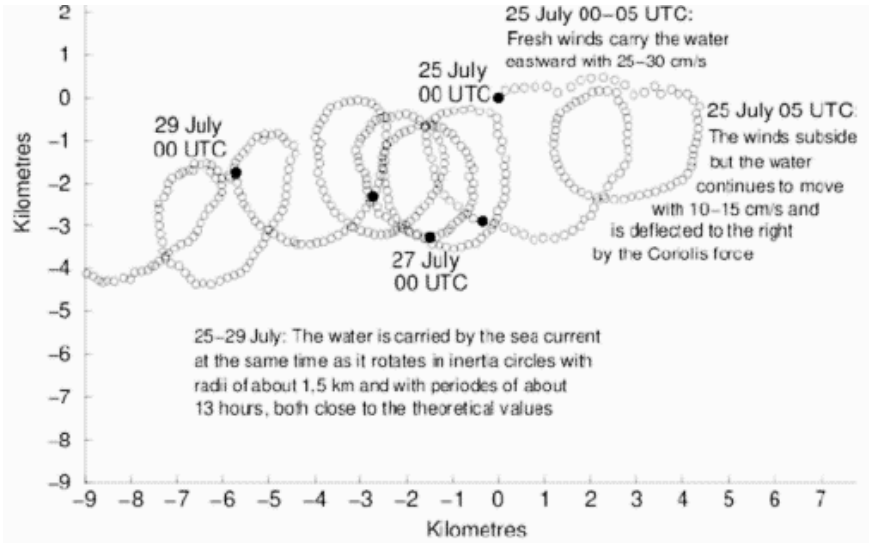

Fig.7. A buoy at sea executing inertial motion [3], [4]

CONCLUSION

Quantitative treatment (algebraically as well as with numerical magnitudes) helped decide whether inertial forces should be considered or can be ignored in a particular situation. Application to geography-related problems supports a deeper understanding in both subjects. As indicated by the results of a short quiz, the investigation of the same motion from different points of view made students more conscious of different reference frames.

REFERENCES

1. https://www.youtube.com/watch?v=4IIVfoDuVIw
2. V. I. Arnold: *Mathematical Methods of Classical Mechanics*, Springer-Verlag, New York, NY, 1978
3. A. Münchow: *Geophysical Fluid Dynamics*, University of Delaware, Newark, 2005
4. A. O. Persson: The Coriolis Effect: Four centuries of conflict between common sense and mathematics, History of Meteorology **2**, 1, 2005
5. http://www.cleonis.nl/physics/phys256/inertial_oscillations.php

CONSTRUCTION OF A LOW-BUDGET QUADROCOPTER AND DESIGN OF A SIMPLE MEASURING MODULE APPLICABLE FOR ATMOSPHERIC MEASUREMENTS

Á. Bordás
Bolyai High School, Senta, Serbia, bordas.arpad@gmail.com

ABSTRACT

During the past school-year a low-budget quadrocopter was constructed at the Bolyai High School. After successful test flights the quadrocopter was equipped with a simple onboard measuring module which contains air pressure, temperature, and humidity sensors, a GNSS module and a data logger. Vertical profile measurements were done in rural and urban areas with the aim of understanding land-atmosphere interactions during different stability conditions, as well as to extend our knowledge about the climate modification effects of cities, which is useful for urban planning strategies.

INTRODUCTION

UAVs (Unmanned Aerial Vehicles) are useful tools in a number of different engineering and scientific disciplines. Through their use, it is possible to test and evaluate new ideas in the fields of navigation, real-time systems, flight control, robotics, as well as environmental monitoring and measuring. A quadrocopter is a type of UAV that is lifted and propelled by four rotors. It uses two pairs of identical fixed pitch propellers, two clockwise and two counter-clockwise. By the independent variation of the speed of each rotor it is possible to control the flight of the UAV.

During the past (2014-2015) school-year the group of Bolyai High School (BHS) students constructed a low-budget quadrocopter and developed an onboard measuring module suitable for atmospheric measurements. The aim of this paper is to the describe characteristics of the BHS quadrocopter and to introduce the measuring module designed by our students. Results of the low altitude profile measurements done during the PABLS 15 (Pannonian Atmospheric Boundary Layer Studies) campaign [1], as well as Urban-Path project [2,3] are also presented.

THE QUADROCOPTER AND THE MEASURING MODULE

Due to limited budget, our aim was to build a multicopter suitable for atmospheric measurements that was as cheap as possible. The frame was made of an aluminium rod, the legs were superflat. The constructed quadrocopter operates using medium-priced hardware (ArduPilot flight controller, 30 A rotation speed controllers, 1000 kv brushless motors and GPS compass). An old radio controller designed for model airplanes was modified; the kHz band radio was replaced with a 2.4 GHz radio system. After tens of hours of practicing on a simulator, the first test flights were performed on the local football field (see Fig.1.). During the test flights we revealed that the quadrocopter can fly up to 20 minutes with a 5000 mAh battery.

Fig.1. Test flight, February 2015

After the successful test flights the students designed a simple measuring module. The module includes Sparkfun's air pressure (MPL3115A2), temperature (TMP102) and humidity (HTU21D) sensors, MicroElektronica's GNSS (Global Navigation Satellite System) click, as well as a simple data logger including a micro SD card. The measuring module was housed in a plastic box and attached to the copter's frame. The measuring module is shown in Fig.2.

Fig.2. The measuring module housed in a plastic box -
data logger with GNSS click (left) and the set of sensors (right)

THE PABLS 15 CAMPAIGN AND THE URBTA-PATH PROJECT

The PABLS 15 campaign [1] was organized at the Szeged Airport (Hungary) in July, 2015. During the campaign the group of students worked with the team for the direct sounding devices. Beside the multicopter soundings [4] the students got an insight into tethered (see Fig.3.) and free balloon soundings. Vertical profile measurements were done with the idea to understand land-atmosphere interactions during different stability conditions. Fig.4. shows characteristic daytime and nighttime temperature profiles obtained using the BHS quadrocopter close to the grassy runway.

Fig.3. Students are performing the tethered balloon measurements during the PABLS 15 campaign (Szeged Airport, July 2015)

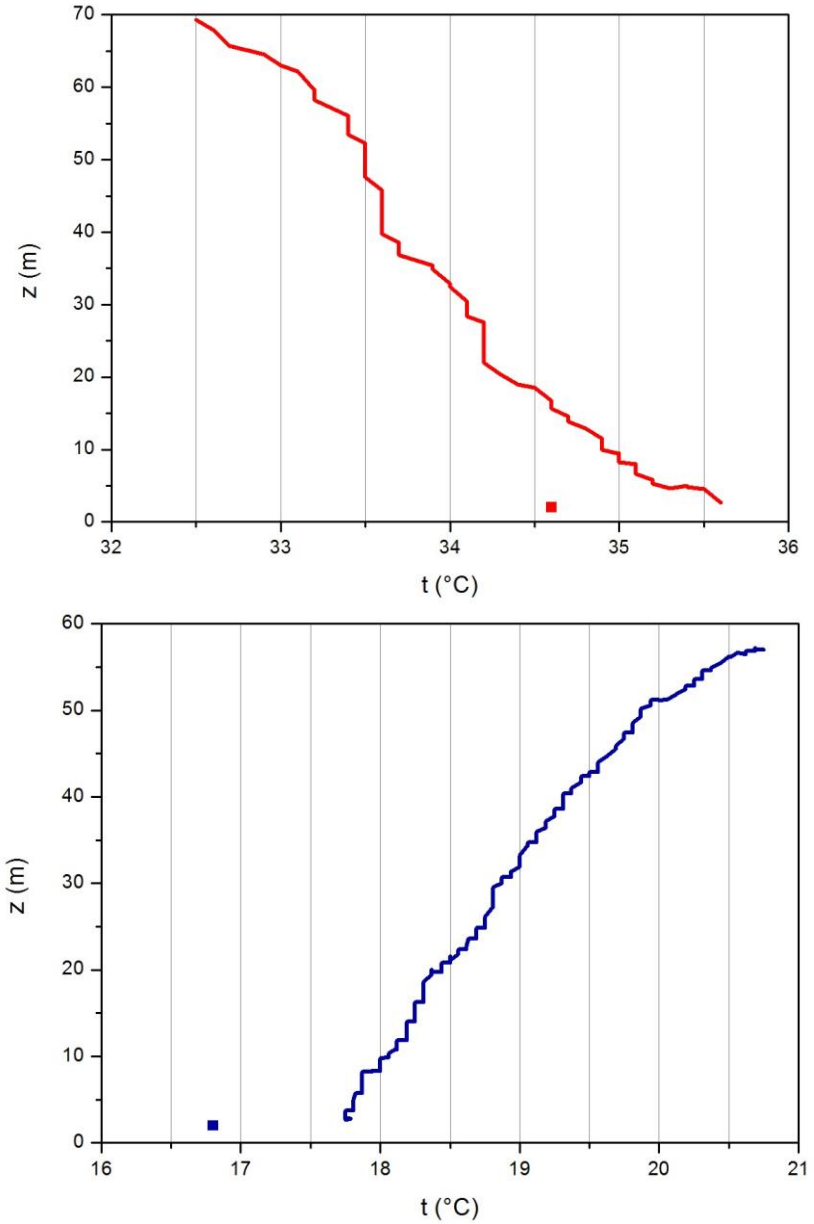

Fig.4. Daytime (red – 13.30 local time, 7th July) and night time (blue – 03.57 local time, 16th July) temperature profiles. Squares indicate temperatures measured at the ground station

Climate modification effects of the cities are very significant and affect many people. The aim of the Urban-Path project [3] was to monitor heat generated by the cities of Szeged (Hungary) and Novi Sad (Serbia) using measurement networks. In both cities more than 20 stations were installed. The spatial resolution of the stations provided high-resolution maps of the urban heat island [5]. Several high school students joined the Urban-Path project team. Vertical profile measurements were performed close to the urban meteorological stations. Differences between the day urban canyon and rural area temperature profiles are presented in Fig.5. Contrary to the rural data, the temperature increases slightly with height in the urban canyon.

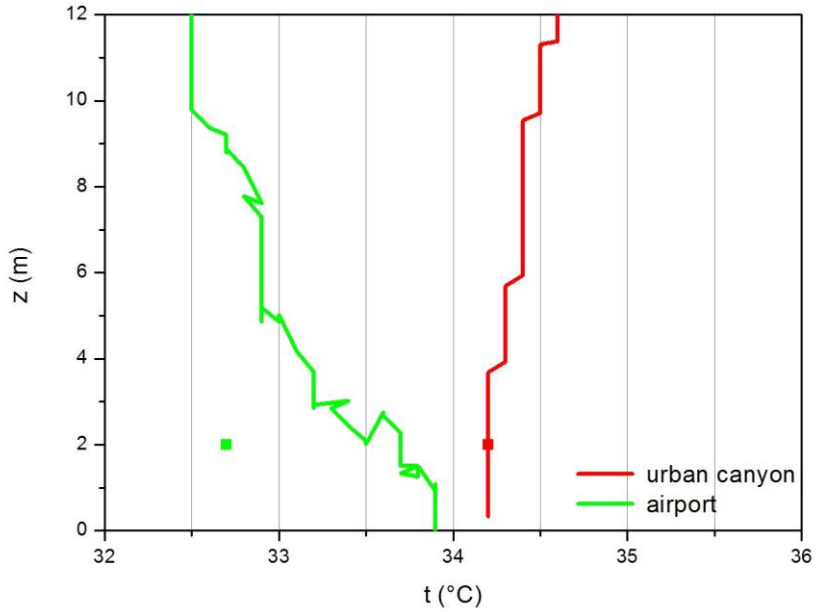

Fig.5. Raw temperature data obtained on July 6th in Szeged
urban canyon (15.37 local time), and at the Szeged Airport (17.27 local time)

FURTHER PLANS

The next step in the development of the BHS multicopter is the installation and testing of the autopilot and improved safety pilot systems. The modified version of the measuring module attached to the DJI Phantom quadrocopter will be used for profile measurements during the Dry Andes Research Program [6].

ACKNOWLEDGMENTS

The author wishes to thank Alexandra Apró, Róbert Boros, Márk Dobó and Tamás Kiss for their work, as well as Burkhard Wrenger (OWL University of Applied Sciences, Germany) and Zoltán Istenes (Eötvös Loránd University, Hungary) for discussions and their suggestions.

REFERENCES

1. J. Cuxart, T. Weidinger, G. Simó, B. Wrenger, A.Z. Gyöngyösi, D. Tátrai, Z. Istenes, B. Matjačić, Z. Nagy, Á. Bordás, A. Kircsi, J. Józsa: Pannonian atmospheric boundary layer studies (PABLS): some findings of the 2013 and 2015 campaigns, GEWEX workshop on the climate system of the Pannonian Basin, Osijek (Croatia) 2015.
2. J. Unger, S. Savić, T. Gál, D. Milošević: *Urban climate and monitoring network system in Central European cities*, University of Novi Sad – University of Szeged, 2014.
3. http://en.urban-path.hu
4. B. Wrenger, Á. Bordás, J. Cuxart, G. Simó, T. Weidinger: Multicopter measurements in the PABLS 15 campaign, GEWEX workshop on the climate system of the Pannonian Basin, Osijek (Croatia) 2015.
5. J. Unger, T. Gál, Z. Csépe, E. Lelovics, Á. Gulyás: Development, data processing and preliminary results of an urban comfort monitoring and information system, Időjárás, **119**, 307, 2015.
6. http://atacama.expedicio.eu/en/

OBSERVATION OF THE DRYING PROCESS IN SECONDARY SCHOOL

Á. Szeidemann[1], Á. Cs. Bodor[2], M. Juhász[1]
[1]Eötvös József Secondary School, Tata, Hungary, szeidiak@freemail.hu
[2]Eötvös Loránd University, Institute of Physics, Budapest, Hungary

ABSTRACT

Some years ago we built a solar dryer during an extracurricular class. Although we had no opportunity to analyse the drying procedure itself, with the help of students we did some experiments and measurements associated with the device. In latter works we used an electric dryer to physically capture the drying by eliminating the environmental effects. We made a series of experiments that are comprehensible in high school. We measured mass reduction of different fruits due to the loss of water over time and compared our results – which resembled the evaporation of a fluid consisting of two constituents – with the literature. A statistical model has been derived to demonstrate the drying.

INTRODUCTION

Some few years back in our school [Eötvös József Secondary School] extracurricular lectures ran on environmental physics, especially focused on environmental flows and solar energy. Related to the latter topic, former students built a solar dryer. They also monitored how it is functioning and made measurements with it. This work – besides raising the motivation of students – has succeeded in an educational point of view by showing it is capable of synthesising the notion of energy and it made possible for students to put abstract conceptions and quantities into use (e.g.: power, efficiency, luminosity).

In the last two years a new research subject adaptable in secondary schools has come into sight connected to the solar dryer. It is plausible to study the process of drying itself instead of the characteristics of a drying machine. The subject has an extended technical literature, but this ought to be made comprehensible for students. In the present article we are to show a train of thought on how the description and measurements are made comprehensible to students. We also show the resemblance of fruit drying and the evaporation of two-constituent compounds and introduce a toy model using dices to demonstrate evaporation.

INSTRUMENTS AND MEASUREMENTS

To describe drying quantitatively we had to work out a measurement procedure which is reproducible. A solar dryer is not suitable for this as it does not fulfil the criteria that the power density required for the loss of water should be constant in time. To exclude this and other environmental effects we obtained an electric dryer.

As a subtask we can compare the two devices by their evaporating efficiency. This quantity is defined arbitrarily and could be calculated from measurement data. A possible definition to this efficiency could be the following:

> *the ratio of the energy needed for a certain amount of water to evaporate from a standardized pot in an hour and the energy used during the process.*

In our case, we used a Petri dish (9.5 cm diameter) as the pot and we filled it with 50 g of water. The energy used by the electric dryer could be calculated from its power, while in the case of the solar dryer it is to be calculated from solar radiation and the effective size of the solar panel. Our measurements showed that the evaporating efficiency of the electric dryer is $\eta_{electric} = 2.5\%$ and the same for the solar one is $\eta_{solar} = 0.3\%$.

During our measurements with the electric dryer we registered the mass of the fruits (apple and banana slices) in the dryer over time. For this, we used a kitchen scale due to the dimensions of the dryer.

Measurements were also made on evaporation. In these cases - again - the mass of a compound of two constituents was registered over time. With a sugar-water compound being the subject of such experiment we used the above set-up due to time it requires to evaporate (we had to speed up the process to fit a double-length class), but when we investigated the evaporation of a paraffin-oil and pentane as a compound we used an analytic balance instead, because the time required was much shorter than in the case of sugar-water.

ANALYSIS OF DATA

There are several mathematical models that describe the drying of sliced vegetables and fruits. It is usual in food engineering articles covering the subject to compare these models to their measurements and use the model that fits the data better. For an example Akpinar et al., 2006 in [1], Akpinar, 2006 in [2] or Diamante and Munro, 1993 in [3] have gathered some of the models to choose the best one describing their measurement data. Table 1 shows the collection of models that are widely used.

Table 1. Mathematical models used to describe drying. This table is an excerpt from [1]

Mathematical models widely used to describe the drying kinetics (Akpinar, Bicer, & Midilli, 2003; Akpinar, Bicer, & Yildiz, 2003; Akpinar et al., 2003a; Ertekin and Yaldiz, 2004; Günhan et al., 2005; Togrul and Pehlivan, 2003; Yaldiz and Ertekin, 2001)

Model no	Model name	Model
1	Newton	$MR = \exp(-kt)$
2	Page	$MR = \exp(-kt^n)$
3	Modified Page (I)	$MR = \exp[-(kt)^n]$
4	Modified Page (II)	$MR = \exp[(-kt)^n]$
5	Henderson and Pabis	$MR = a \cdot \exp(-kt)$
6	Logarithmic	$MR = a \cdot \exp(-kt) + c$
7	Two-term exponential	$MR = a \cdot \exp(-kt) + (1 - a)\exp(-k\,a\,t)$
8	Wang and Singh	$MR = 1 + at + bt^2$
9	Verma et al.	$MR = a \cdot \exp(-kt) + (1 - a)\exp(-g\,t)$

From this we will use the Modified Page (I) model because it gave the best fits – among the models mathematically comprehensible for an average high school student – with our experiments. For the description we will use quantities generally used in food engineering. These are: moisture content (on wet basis) and moisture ratio. M is used to denote the former one, while MR the latter. These quantities depend on time and are defined as:

$$M(t) = \frac{m_w(t)}{m(t)}, \tag{1}$$

$$MR(t) = \frac{M(t) - M_e}{M_i - M_e}. \tag{2}$$

In the formulas above m(t) denotes the mass of the sample, $m_w(t)$ the mass of water contained in the sample while M_i stands for the initial moisture content and M_e for the one in equilibrium, given the conditions (temperature and relative humidity in the dryer).

One could see that to determine the moisture ratio additional information is needed besides the moisture content, and this is the weight of dry matter in the sample. This will be marked with m_d. Equivalent to this is either the initial or the equilibrium moisture content. Unfortunately, neither of these could be measured with standard high school equipment, so a good guess on either of them is needed. In our case the guess is the data available in [4] to determine M_i for banana and apple – the fruits measured. Under the condition that m_d is constant, we see that $m_w(t)=m(t)-m_d$. Also, we can write the constants M_e and M_i with the masses:

$$M_e = \frac{m_w(\infty)}{m(\infty)} = \frac{m(\infty) - m_d}{m(\infty)}, \tag{3}$$

$$M_i = \frac{m_w(0)}{m(0)} = \frac{m(0) - m_d}{m(0)}. \tag{4}$$

The equation we will use (Modified Page model) to fit our data is the following:

$$MR(t) = \exp[-(kt)^n]. \tag{5}$$

This could be linearized easily in the following way:

$$\log(-\log(MR(t))) = n\log(k) + n\log(t). \tag{6}$$

This equation easily fits our data from experiments for given time intervals. We will discuss the results for both drying and evaporation in the upcoming sections.

DRYING PROCESS

The data from measurements with apple and banana and the result of the analysis described above are shown on Figs.1 to 3.

In Fig.3. deviations from linear could be seen at the high time values for both fruits. We suppose that the model we used lacks the correct description near the equilibrium. The fact that the concrete amount of dry matter is unknown also matters, especially at the equilibrium. Other than this, the linear fitting seems to be correct for most of the time with $R^2 = 0.997$ and the parameters are close to each other, $n \sim 1.45$ and $k \sim 0.01$.

Up to this point experiments and mathematical models were discussed, but as seen, we left out the actual physics of drying. This is because it is usually described by diffusion and other transport-equations. The different boundary and other conditions lead to the different mathematical constructions. This is a rather complex and difficult topic to discuss, even on extracurricular class, so we made a physical approximation and claimed that evaporation could be seen as a similar physical process to drying.

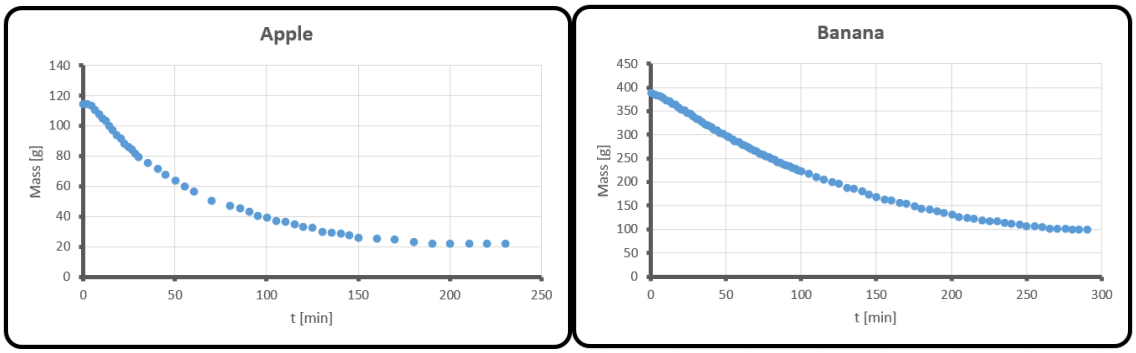

Fig.1. Mass of fruits over time: Left panel: apple. Right panel: banana

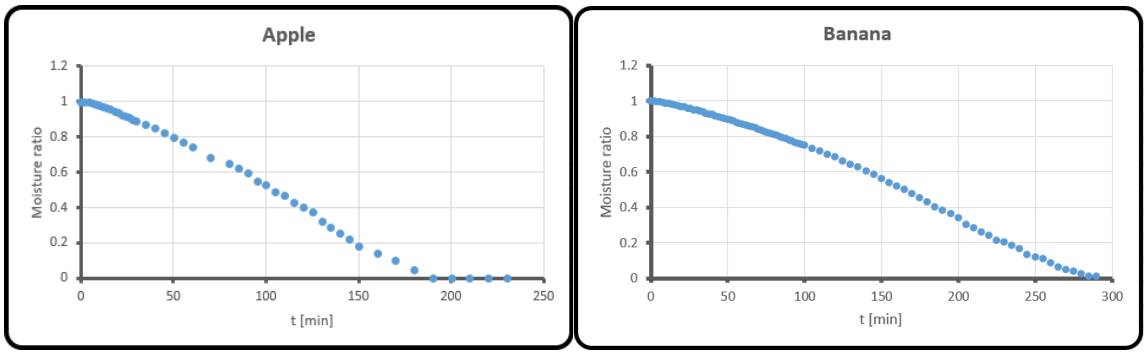

Fig.2. Moisture ratio of the fruits over time: Left panel: apple. Right panel: banana

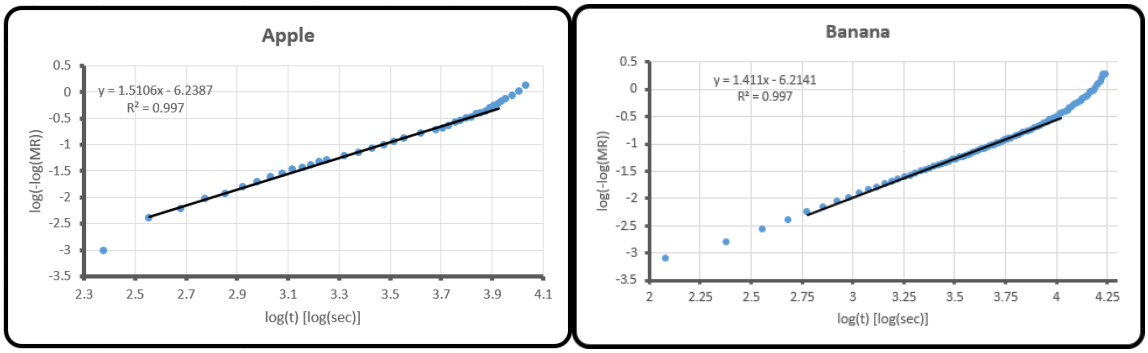

Fig.3. Values calculated using eq. (6), the line fitted with its parameters:
Left panel: apple, n = 1.5106, k = 0.0160. Right panel: banana, n = 1.4110, k = 0.0122

EVAPORATION

Experiments were made on the evaporation of two-constituent compounds – one of which is volatile (e.g. water) and the other is non-volatile – to physically model the drying process. The reason for this is that evaporation is a less complex phenomena taught on regular physics classes. The closest estimation of fruits (e.g. banana and apple) with two components is a sugar-water compound. In this physical model sugar represents the dry matter in fruits. The moisture content and moisture ratio was calculated for this compound from mass measured over time during the evaporation. The initial moisture content was 80%, which is a good generalisation for the fruits used previously. It is to be mentioned that the experiments with this compound were carried out with the same set-up as the one used in the case of fruit drying (an electric dryer on top of a kitchen scale), because the evaporation in open air took much more time than available for a double class (which is 120 minutes).

We investigated another compound, consisting of organic materials, paraffin-oil and pentane. Here, pentane was the non-volatile compound. This experiment is useful because in general, organic materials evaporate much faster, so in this case the set-up with the dryer was not needed to fit into the time of a class. An analytic balance and a petri dish was used instead to proceed with the measurements. The results, - extracted by the same analysis as in the case of drying before - can be seen in Fig.4.

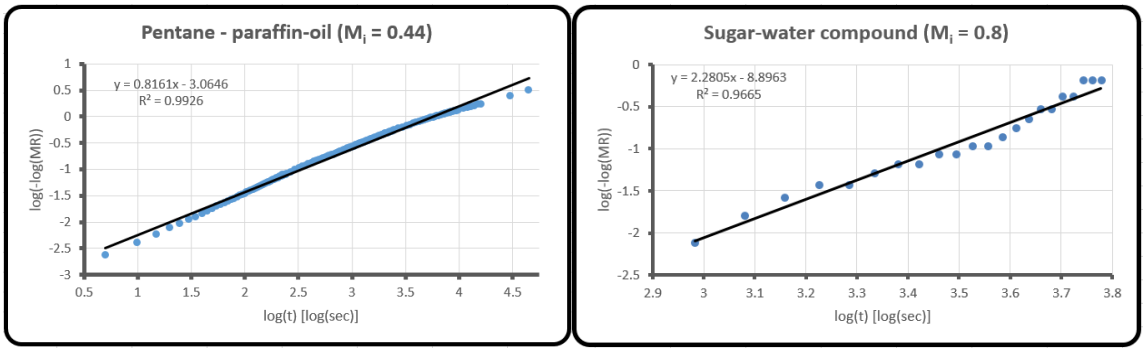

Fig.4. Values calculated using Eq. (6) for the description of evaporation, and the line fitted with its parameters: Left panel: pentane – paraffin-oil, n = 0.8161, k = 0.0233. Right panel: sugar-water, n = 2.2805, k = 0.0202

As seen in the figure, the mathematical model fits our data on evaporation well, in the case of the pentane – paraffin-oil even better than in the case of fruits. We think it is important that the dry matter content of the samples is known exactly this time, so this does not bring another uncertainty in the data.

To sum up: an approximation – a physical approximation – was made that the evaporation is similar to drying, and we described this with the same mathematical model successfully.

A TOY MODEL OF EVAPORATION WITH DICES

Investigating evaporation further, a toy model (or dice model, as it requires the use of dices) had been derived and was used successfully as a demonstration for this phenomena. To introduce this, we will need dices of two colours. Let us say that dices of one colour (these will be referred to as white dices from now on) represent the volatile component of a two-constituent compound (e.g. water), while the dices of the other (these will be referred as the red ones) represent a non-volatile component, or going further we could say that these stand for the dry matter in a given fruit. The ratio of the white dices to all of the dices represents a given initial moisture content, M_i. After this some dices are to be put on a table, which represents the surface of the compound or the fruit. After this initialisation we roll the white dices on the "surface" and if one of them is a six, we take that one out of the game – this is to be concerned as the loss of weight over time. This game or toy model supposes a constant surface area, so after taking dices out of the game one has to "refill" the table. This could happen in different ways, representing different physical conditions. Examples: one could refill from under the table with white and red dices in a way the ratio of whites and reds (taking into account both the dices on and under the table) remains constant, or this could be done with only white dices (see Fig.5.), this way the ratio will depend on time. After enough turns in the game, there will be no white dices left on the surface, so it ends.

This game could be introduced in high schools very easily as it demonstrates evaporation in a more engaging way than most books do. Also it is possible to analyse a game with the same method as used above for drying and evaporation. To exemplify this, Fig.6. shows data from a class where this model was introduced and tried with students.

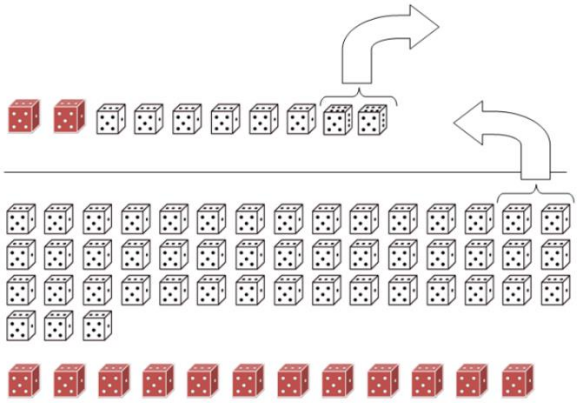

Fig.5. Example for the toy model introduced. It shows a possible pattern for replacing white dices on the surfaces.

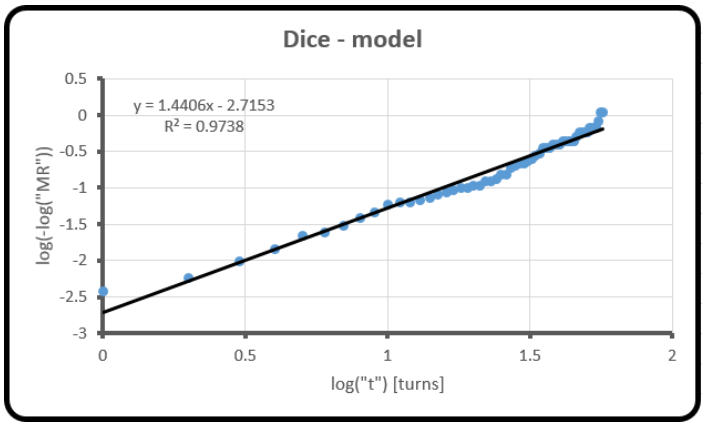

Fig.6. An example to show that the same data analysis could be done in the toy model.

CONCLUSIONS

We have shown a possible way of introducing supplementary material on fruit drying in high school physics (or other science) classes. This could prove a very rewarding area as it is possible to include device development (building a solar dryer), experiments and measurements (to explore the characteristics of a given device, or to investigate a physical process), data analysis with given mathematical models, linearization of equations, analogous thinking. It could also serve as an entry point for more advanced students into the topic of diffusion, or even model building with differential equations. We have also derived a new toy model of evaporation with dices. This proved to be a powerful demonstrational tool as it caught the attention of students besides those who were already interested.

REFERENCES

1. E. Kavak Akpinar, Y. Bicer, F. Cetinkaya: Modelling of thin layer drying of parsley leaves in a convective dryer and under open sun, J. Food Eng. **75**, 308, 2006
2. E. Kavak Akpinar: Mathematical modelling of thin layer drying process under open sun of some aromatic plants, Journal of Food Engineering **77**, 86, 2006
3. L. M. Diamante, P. A. Munro: Mathematical modelling of the thin layer solar drying of sweet potato slices, Solar Energy **51**, 271, 1993
4. http://www.britannica.com/topic/fruit-processing
5. M. R. Queiroz, S. A. Nebra: Theoretical and experimental analysis of the drying kinetics of bananas, Journal of Food Engineering **47**, 127, 2001

A FEW YEARS EXPERIENCE OF THE ENERGY CONSUMPTION OF A HIGH SCHOOL IN BUDAPEST

Istvan Gärtner
Árpád Secondary Grammar School, Budapest, Hungary, gartner.istvan@arpad.sulinet.hu
Physics Education PhD program, Eötvös University, Budapest

ABSTRACT

I analyzed the consumption of electrical and heating energy based on the data of meters between April 2012 and March 2015 in Arpad Secondary Grammar School in Budapest. In my presentation I summarize the experiences which were obtained from the data. First I compare and explain the consumption of energy between the years and between the different periods of the years. I determine the amount of energy per person and per student groups too, and with a little calculation I interpret the results. After another short calculation I outline whether is it worth for our school to change heating mode. Finally I suggest potential solutions for reducing the consumption of energy which may lead to savings for the school.

INTRODUCTION

The Arpad Secondary Grammar School (Fig.1.), located in the northern part of Budapest, was founded in 1902. From 2012 it has 22 classes, the number of students is about 700.

The building of the school is 75 years old, it has central heating and it is provided with electrical energy by Budapest Electricity Works. We cannot say this building is an energy saving one because of the bad status of the doors and windows and the outdated heating and electrical system. There is no air-conditioning, and both the heating and electric providers are independent from the school.

Fig.1. Árpád Secondary Grammar School in Budapest

AIMS OF THE WORK

The aims of the investigation were to collect and to present those two types of energy data (electrical and thermal energy) which are most important in the field of education in the school. After analyzing them it will be shown through an example taken from everyday life how the data can be made understandable for high school students. Based on the interpretation some options for energy saving will be suggested, too.

DATA FOR ENERGY CONSUMPTION

All energy data – presented in GJ unit – were read in every month from the meter readings between April 2012 and March 2015. The annual (Fig.2.) and the quarterly data charts below (Figs. 3.-5.) show the consumption of energy.

EXPERIENCES

On the annual chart (Fig.2.) it is noticeable that in the first and in the third year the ratio of electrical and thermal energy is about one quarter, but in the second year it is only about one third. The reason is that the temperature of the winter in 2013-2014 was about 2.5 centigrade higher than the hundred-year average so though the consumption of electrical energy increased a little, but the consumption of the thermal energy decreased by much more.

The other information is – as mentioned before – that the consumption of electrical energy increased. The value was higher not only in the second but in the third year. One possible explanation for this was the creation of a new information technology room which operated throughout the whole school year.

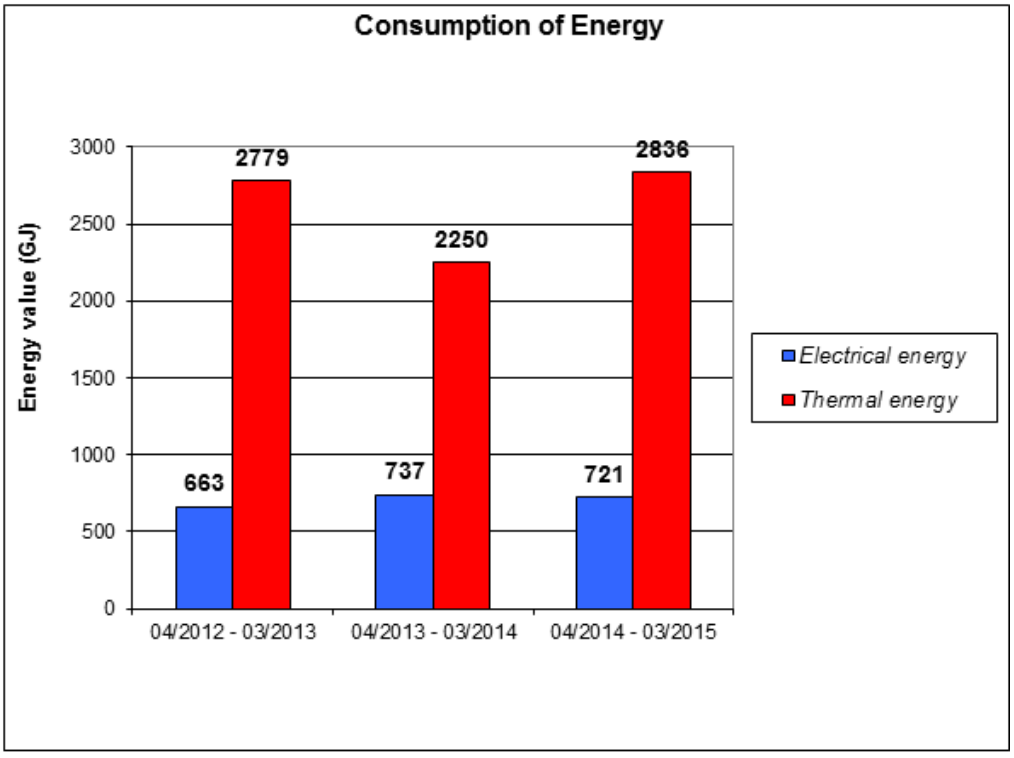

Fig.2. Annual data chart of energy consumption

The next three graphs (Figs.3.-5.) show the quarterly data charts. On all three graphs the periodicity can be seen and from left to the right we can separate the seasons, too. Probably it is not surprising that in the third and in the fourth quarters the thermal energy is 5-7 times more than the electrical energy.

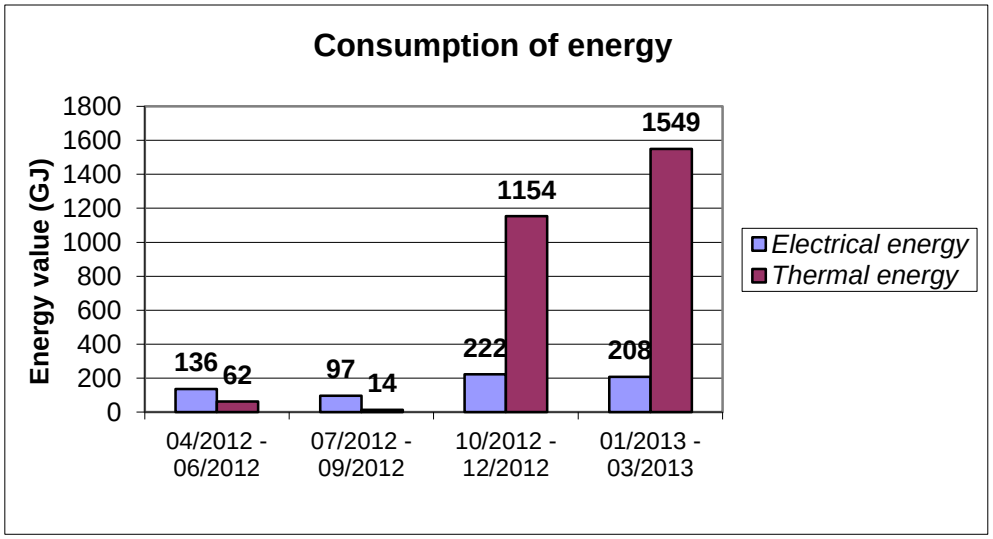

Fig.3. Quarterly data chart of energy consumption – 2012-2013

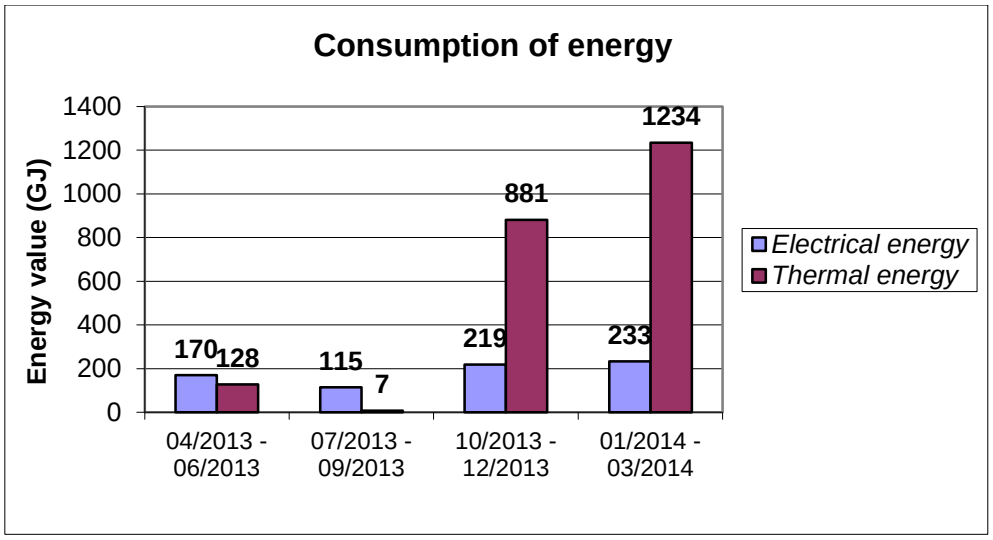

Fig.4. Quarterly data chart of energy consumption – 2013-2014

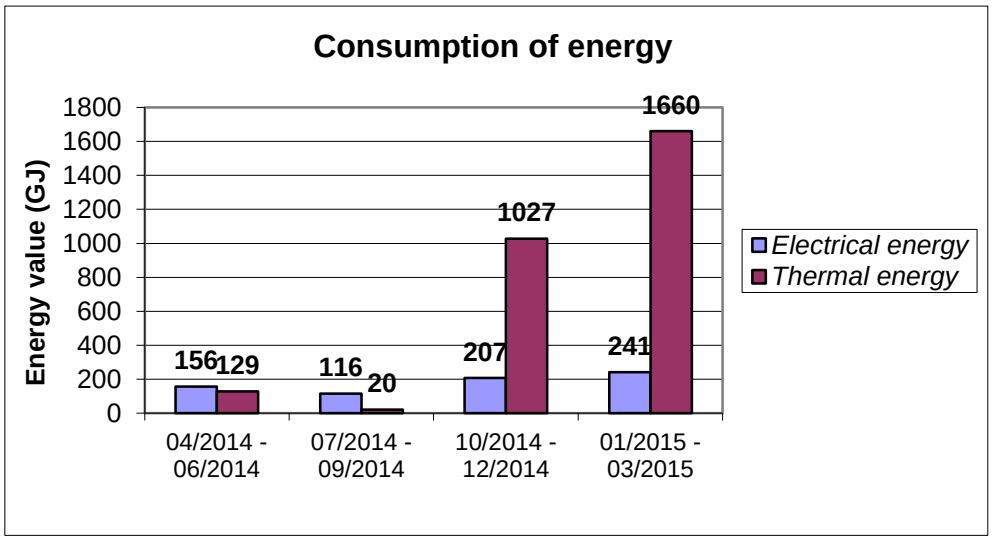

Fig.5. Quarterly data chart of energy consumption – 2014-2015

On the following diagram (Fig.6.) I show the cumulative annual energy values per capita. It is about 5 GJ on average per person.

I also calculated the price of this energy quantity, the value of it is about 100 Euros in Hungary in 2015.

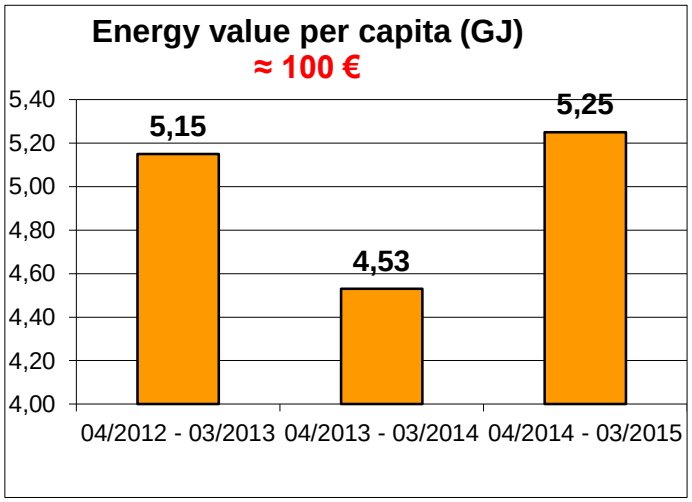

Fig.6. Annual energy consumption per capita

To make the data of the chart understandable for everyone I try to solve a calculation problem which is as follows:

The human body can burn 200 kilocalories in 10 minutes on an exercise bike in the case of a uniform load. The efficiency of the human body is 0.25 [3]. Calculate how much work can be done by a high school student and a class of 30 students in half an hour on it!

$$Q = 3 \cdot 200 \text{ kcal} = 600 \text{ kcal} = 2520 \text{ kJ} = 2.52 \text{ MJ}$$

$$\eta = 0.25$$

$$W = \eta \cdot Q = 0.25 \cdot 2.52 \text{ MJ} = 0.63 \text{ MJ}$$

$$\Sigma W = 30 \cdot 0.63 \text{ MJ} = 18{,}9 \text{ MJ}$$

The solution of the task is 0.63 MJ – assuming that the efficiency of the human body is about 0.25 [3] – and 18.9 MJ if we consider a class with 30 students. These values become clear if we assign such content to them which is in connection with the everyday life.

In our school the rooms are lit by fluorescent lamps, in each room the total power for lighting is 900 W. Let's assume that the whole work of the class produces electric energy.

$$\Sigma W = 18.9 \text{ MJ} = 18900 \text{ kJ} = 18900000 \text{ J}$$

$$P = 900 \text{ W}$$

$$t = \Sigma W / P = 18900000 \text{ J} / 900 \text{ W} = 21000 \text{ s} \approx 5.83 \text{ h}$$

In this case the energy produced by the whole class is sufficient for less than 6 hours. It means that 30 high school students with hard training cannot produce the amount of energy that a school needs for the lighting of a room in the daily teaching.

It is interesting to determine how much time a high school student needs to produce the annual energy consumption. I used the data of the chart "Annual energy data consumption per capita" (Fig.6.) and I calculate with the mentioned 5 GJ average value. I also used the result

from the first calculation problem which showed how much work can be done by a high school student riding on an exercise bike in half an hour. It was 0.63 MJ.

$$\Sigma E = 5 \text{ GJ} = 5000 \text{ MJ}$$

$$W = 0.63 \text{ MJ}$$

$$t = \Sigma E / W \approx 7936 \text{ half an hour unit} \approx 165 \text{ day (without interruption)}$$

I think the solution of the problem is hard to believe, but it should be clear from this result as well that the energy that we can produce in a mechanical way is only a fraction of the quantity that a school needs for its operation. If we try to compare the energy produced by mechanical work with the annual energy consumption, the difference is about two orders of magnitude.

In the light of this striking result it is worth thinking about what the options of a high school for energy saving can be. Even students know that switching off the unnecessary lights will not cause significant saving so we have to look for more efficient solutions.

One possibility would be to change the heating system from central heating to gas heating. Knowing and using the different parameters of gas heating [2],[4] which are typical for traditional gas boilers, after a short calculation we can realize that the costs would be only about 70% of the current costs but the implementation would require serious investment.

$$\Sigma Q = 2800 \text{ GJ (Fig.2.)} = 2800000 \text{ MJ}$$

$$\eta = 0.85$$

$$L = 34 \text{ MJ/m}^3$$

$$V = \Sigma Q / (\eta \cdot L) = 2800000 \text{ MJ} / (0.85 \cdot 34 \text{ MJ/m}^3) \approx 97000 \text{ m}^3 \text{ (price of it is about 32000 Euros)}$$

The other and maybe more viable way for us would be to use alternative energy sources [1], the most feasible of these seems to be the photovoltaic system.

This photo (Fig.7.) was taken in another secondary school – Fasori Gimnázium in Budapest – where the system has been working since April 2015. According to the descriptions – that the school got from the manufacturer – it can produce about 30 MWh = 108 GJ, mainly electric energy. It covers the whole energy demand of the lighting and it is about a quarter of the total electric energy. The school won 85% of the investment costs in a tender opportunity. This solution can be reachable in the future for our school, too [4].

Fig.7. Photovoltaic system in Fasori Gimnázium in Budapest

CONCLUSIONS

In physics teaching the concept of energy is very important. Students meet both with conventional and renewable energy sources during their physics studies. In my teaching process I only mention the topic of this presentation and try to interpret the charts and the results of the calculation problems first in the eighth grade. The main focus of the whole theme of energy saving is in the tenth and eleventh grade where besides the correct interpretation students can complete their knowledge with more calculations and measurements which are in connection with concrete devices (e.g. solar cells).

In this presentation first I summarized and presented the thermal and electrical energy consumption of our school in the last three years. I tried to interpret itwith an example where a comparison was made to the human power. Although it had a surprising and thought-provoking result, it can provide an opportunity to our high school students to recognize that the energy saving will be vital in their future life. On the other hand as a physics teacher I tried to adumbrate some possible solutions for energy saving in my school, too, but all my activities were directed at the didactic task to raise students' awareness of the importance of the problem.

Finally anybody can ask what can be implemented from these? I think the main purpose that students' thinking can develop is achievable. The realization of energy saving ideas needs not only much money but the human will, too. I have 9 more years to retirement and I would like to see it as an active teacher. So I hope….

ACKNOWLEDGEMENTS

I want to express my special thanks to Professor Adam Kiss who supported me with his remarks, ideas and suggestions. I am grateful for the collected energy data to my working-place (Fig.1.), too.

REFERENCES

1. https://secondlawoflife.wordpress.com/tag/energy-efficiency-human-body/
2. J. Goldemberg: *Energy: what everyone needs to know*, Oxford University Press, New York, 2012
3. https://www.eia.gov/todayinenergy/detail.cfm?id=14051
4. R. Wengenmayer, T. Bührke: *Renewable Energy*, WILEY-VCH, Weinheim, 2013

SIMPLE MODEL FOR THE ENERGY SUPPLY OF A STAND-ALONE HOUSE USING HYBRID WIND–SOLAR POWER SYSTEM

Tamás Beke
Our Lady Catholic Grammar School, Kalocsa, Hungary, bektomi@gmail.com
Physics Education PhD Program, Eötvös University, Budapest

ABSTRACT

A research project for secondary school students involving both physical measurements and modelling is presented. The problem to be solved is whether and how a typical house can be supplied with energy off-grid, based entirely on renewable energy sources, more specifically, on solar and wind energy, while using relatively simple devices, namely, photovoltaic modules, wind turbines and accumulators. Our students carried out a long term measurement series in order to assess typical energy consumption of houses. Further, the number of solar modules and wind turbines and the necessary accumulator capacity was estimated.

INTRODUCTION

Renewable energy sources are becoming increasingly important in energy supply. Their contribution covered an estimated 19% of the global energy consumption in 2011 [1]. The application of the renewable energy resources helps to reduce global greenhouse gas emission and mitigate global warming [1, 2, 3]. Due to their significance and perspective, it is desirable to give renewable energy sources an appropriate share in physics teaching. In this paper a related research project designed for and accomplished by secondary school students is described. Our students examined the role of the renewable energy sources and the behaviour of an off-grid hybrid wind-solar model system using elementary concepts of physics. In this model electricity was generated by means of photovoltaic (PV) modules and wind turbines, while the electrical energy was stored in accumulators. A quite similar model was discussed in [4].

We can make the traditional lessons more colourful with different project tasks. The well-planned project tasks augment students' knowledge in the particular topic and make students more motivated in learning that subject. According to my experience the most effective tasks were carried out in pairs or groups with the teacher's guidance, as well as in this project.

Our 'Renewable energy sources: stand-alone house with hybrid wind-solar power generator' project has been carried out in three stages. For the first stage the daily energy consumption of an average house was investigated. Energy consumption of electric home appliances and energy consumption of air conditioner and heating energy were monitored separately. During the project, which lasted for 2 years (from 2012-Oct-1 to 2014-Oct-1), the students measured the daily energy consumption of their households. The wind speed and the sunlight were also monitored. For the second stage we developed a mathematical model for an off-grid house with hybrid wind–solar power generator and accumulator system. For the third stage a computer simulation program was developed, based on the mathematical model and the data collected by students. This programme enabled the simulation of the energy system of an off-grid house. The feasibility of the model was also analyzed; in particular the necessary accumulator capacity was determined. The main purpose of the project was, however, educational.

MODELLING

The model setup is depicted schematically in Fig.1. The parts of the system are the power generating system (photovoltaic modules and wind turbines), the energy storage unit (accumulator system); and the appliances: electric home appliances, electric heating system and cooling system. The solar modules are mounted on the roof.

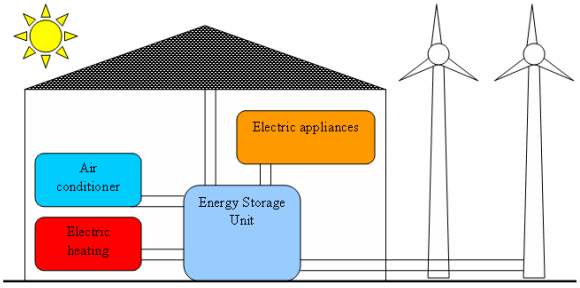

Fig.1. The stand-alone model house with hybrid wind–solar system and energy storage unit

Gathering data

Our 16 - 18 old year students took part in this project voluntarily. The number of students taking part in the project was N=31. Measurements were carried out partly at home and partly in extracurricular afternoon physics classes in team work. Students collected the data of the daily energy consumption of their own houses: the energy consumption of the electric appliances was monitored; the natural gas consumption was monitored by gas meter; the wood and coal burned in furnaces were measured in weighing-machines (scales). The electrical energy consumption of the air conditioner was monitored (estimated) separately from the electric home appliances. The data was gathered by students then we counted the averaged values on a daily basis:

$$E_{total,i} = \frac{A_{ave} \cdot N_{ave}}{N} \sum_{j=1}^{N} \frac{E_{total,i,j}}{A_j \cdot N_j}, \qquad (1)$$

where $E_{\text{total},i}$ is total averaged energy consumption of the model house on ith day, A_{ave} is average floor-space of houses, N_{ave} is the average number of inhabitants in the house, A_j is floor-space of the house of jth student, N_j is the number of inhabitants in the house of jth student, $E_{\text{total},i,j}$ is total energy consumption of the house of jth student on ith day.

In the given 2-year period the average daily electricity consumption per household was 36.08 MJ; the lowest average daily electrical energy consumption was 27.44 MJ and the highest one was 41.89 MJ. (Before doing the project, most of the students could not even estimate the order of the energy consumption of their own home. During the project they learnt to collect, process and analyze data in the long run.)

We monitored the local outside temperature as well as the inside temperature during the project. The wind speed, the air pressure and the sunlight were monitored in every Δt=5 minutes automatically by the local weather station, so these data were available for us.

PV modules

A photovoltaic (PV or solar) cell converts the energy of light directly into electricity by the photovoltaic effect. A photovoltaic module is built from blocks of photovoltaic cells. The power of a photovoltaic module is proportional to the incoming light power [4]. The total energy production of the photovoltaic modules on ith day can be calculated as

$$E_{photov,i} = \sum \eta_{photov} \cdot A_{photov} \cdot I \cdot N_{photov} \cdot \Delta t, \qquad (2)$$

where A_{photov} is the area of one PV module, I is the light intensity (incident solar flux in W/m^2), η_{photov} is the efficiency of the solar module on ith day and N_{photov} is the number of PV modules.

Wind turbines

Wind turbine generates electricity from the kinetic energy of the wind. In our model small (not commercially serialized) wind turbines are used to generate electricity. For simplicity the turbines are assumed to be self-orientating devices. The power output of the wind turbine is proportional to the cross sectional area swept by the rotor and to the cube of the wind velocity [5, 6]. The total energy production of the wind turbines on *i*th day can be calculated as

$$E_{windt,i} = \sum C_{po} \cdot \frac{\rho_{air}}{2} \cdot A_{rotor} \cdot v_{wind}^3 \cdot N_{windt} \cdot \Delta t, \quad (3)$$

where ρ_{air} is the density of air, A_{rotor} is the cross sectional area of rotor, v_{wind} is wind velocity, C_{po} is the power coefficient, and N_{windt} is the number of wind turbines. The density of air is $\rho_{\text{air}}=p \cdot M \cdot R^{-1} \cdot T^{-1}$; where p is the pressure (monitored), T is the absolute temperature of air (monitored), M=0.029 kg•mol^{-1} is the molar mass, and R is the universal (molar) gas constant.

Accumulators

The electricity demand of the model house can change significantly on a smaller timescale. When electrical energy is generated in solar modules and/or in wind turbines, it gets stored instantly in accumulators according to the model assumption. We discussed what size of accumulator capacity ($E_{\text{acc\_max}}$) is suitable for the parameters given in our off-grid system. We must take a battery system large enough to prevent blackouts (total energy loss) in the whole period of the project.

ENERGY INPUT AND OUTPUT AND ENERGY STORAGE

In order to determine the necessary storage capacity of batteries, we studied the energy inputs (produced energy) and outputs (dissipated energy) of the system in detail.

Heat transmission

Temperature difference in any situation results in energy flow into the system or energy flow from the system to its surroundings. The former leads to the heating, the latter leads to the cooling of the system. The total energy flow of heat transmission process on *i*th day is

$$E_{heattr,i} = \sum U \cdot A_f \cdot (T_{out} - T_{in}) \cdot \Delta t, \quad (4)$$

where A_{f} is the free surface area of building, U is the overall heat transmission coefficient, T_{out} is the absolute temperature of ambient air, T_{in} is the absolute inner temperature of the building.

Thermal radiation

The accurate analysis of heat radiation of the system is a complex problem; so we try to construct only an approximate model accounting for thermal radiation. The total energy flow of heat radiation process on *i*th day:

$$E_{rad,i} = \sum \varepsilon \cdot \sigma \cdot A_f \cdot \left(T_{out}^4 - T_{in}^4\right) \cdot \Delta t, \quad (5)$$

where σ is Stefan-Boltzmann constant (σ=5.67•10^{-8} W•m^{-2}•K^{-4}), ε is the overall (average) emissivity of the building.

Heating

Our building is an off-grid system and has electric heating; that is, electric current through a resistor releases heat. The total electrical energy consumption of resistance heating on *i*th day:

$$E_{heating,i} = \sum P_{heating} \cdot \Delta t, \quad (6)$$

where P_{heating} is the electric power of resistance heater.

In the model if the required inside temperature of the building is higher than the actual inner temperature, then we use the electric heating system. If the instantaneous outside temperature is

higher than the required inside temperature of the building in the 'heating season' then it is not necessary to use the heaters, we can warm the interior of the house by opening the windows.

Cooling

If the temperature inside the house is too high (in summer) we can use an air conditioner; it is a device that lowers the air temperature. The cooling process is typically achieved through refrigeration cycles. The total electrical energy consumption of air conditioner on *i*th day:

$$E_{cooling,i} = \sum P_{aircond} \cdot \Delta t, \tag{7}$$

where P_{aircond} is the electric power of the air conditioner.

In the model if the required inside temperature of the building is lower than the actual inner temperature, then we use the air conditioner. If the instantaneous outside temperature is lower than the required inside temperature of the building in the 'non heating season', then it is not necessary to use the air conditioner, we can cool the house interior by opening the windows.

Internal energy

Our building can store energy as internal energy. The internal energy of a macroscopic system at a given temperature is proportional to its heat capacity [7]. The internal energy of model house on *i*th day is assumed to be

$$E_{internal,i} = C_{air} \cdot T_{in,i} + C_{wall} \cdot \frac{T_{in,i} + T_{out,i}}{2}, \tag{8}$$

where C_{wall} is the heat capacity of walls, and C_{air} is the heat capacity of air inside the building.

ENERGY BALANCE

Now the energy balance of the hybrid wind-solar power generating system is considered.

Heating season

It is supposed for the sake of simplicity that in the 'heating season' the internal energy of the model house on *i*th day ($E_{\text{internal},i}$) depends on the internal energy on the previous day ($E_{\text{internal},i\text{-}1}$), the net electric heating on *i*th day (if any), and the net energy flowing in or out of the system by heat transfer ($E_{\text{heattr},,i}$) and heat radiation process ($E_{\text{rad},i}$) on *i*th day:

$$E_{internal,i} = E_{internal,i-1} + \eta_{heating} \cdot E_{heating,i} + E_{heattr,i} + E_{rad,i}, \tag{9}$$

where η_{heating} is the efficiency of the electric heating device. In this model resistance heater is applied, thus η_{heating} is nearly 1 because an off-grid electric resistance heater converts (nearly) the full electric energy into heat. (Some energy is needed by ventilators, if any.)

According to the household's need, the total daily electrical energy consumption on *i*th day is the energy of electric home appliances and electric heating. In the 'heating season' the energy stored in accumulators at the end of *i*th day ($E_{\text{acc},i}$) depends on the energy stored in batteries at the end of the previous day ($E_{\text{acc},i\text{-}1}$), the total electrical energy produced by PV modules ($E_{\text{photov},i}$) and wind turbines ($E_{\text{windt},i}$) on *i*th day, and the total energy dissipated in the electric resistance heater ($E_{\text{heating},i}$) and electric home appliances ($E_{\text{eapp},i}$) on *i*th day:

$$E_{acc,i} = E_{acc,i-1} + E_{photov,i} + E_{windt,i} - E_{heating,i} - E_{eapp,i}. \tag{10}$$

Non-heating season

In the 'non-heating season' the internal energy of model house on *i*th day ($E_{\text{internal},i}$) depends on the internal energy of the house on the previous day ($E_{\text{internal},i\text{-}1}$), the net cooling energy on *i*th day (if any), and the net energy flowing in or out the house by heat transfer ($E_{\text{heattr},,i}$) and heat radiation process ($E_{\text{rad},i}$) on *i*th day:

$$E_{internal,i} = E_{internal,i-1} - C_{cooling} \cdot E_{cooling,i} + E_{heattr,i} + E_{rad,i}\,, \tag{11}$$

where C_{cooling} is the coefficient of performance (COP) of the air conditioner.

According to the household's need the total daily electrical energy consumption on *i*th day is the energy of electric home appliances and air conditioning. In the 'non-heating season' the energy stored in accumulators at the end of *i*th day ($E_{\text{acc},i}$) depends on the energy stored in batteries at the end of the previous day ($E_{\text{acc},i\text{-}1}$), the total electrical energy produced by PV modules ($E_{\text{photov},i}$) and wind turbines ($E_{\text{windt},i}$) on *i*th day, and the total energy dissipated in air conditioner ($E_{\text{cooling},i}$) and electric home appliances ($E_{\text{eapp},i}$) on *i*th day:

$$E_{acc,i} = E_{acc,i-1} + E_{photov,i} + E_{windt,i} - E_{cooling,i} - E_{eapp,i}\,. \tag{12}$$

SIMULATIONS

We used spreadsheet software for the simulations. This method enables the solution of a complex physical (mathematical) problem in a relatively simple way. In the simulations we 'estimated' the energy consumption of a typical house with 4 inhabitants. We tried to choose realistic data for the simulations according to the data gathered by students. Our model house is a hollow rectangular building, with A_{ave}=100 m^2; the dimensions are a=10m, b=10m, h=3m (height), the thickness of walls is d=0.4 m. In Fig. 2. the electrical energy produced by photovoltaic modules and wind turbines can be seen in the 2-year period of project (from 2012-Oct-1 to 2014-Oct-1). The power coefficient of the not commercially serialized wind turbine is C_{po}=0.25, the cross sectional area of rotor is A_{rotor}=4 m^2, the number of wind turbines is N_{windt}=4. The area of one PV module is A_{photov}=1 m^2, the number of solar modules is N_{photov}=100, the efficiency of the solar module is η_{photov}=0.15.

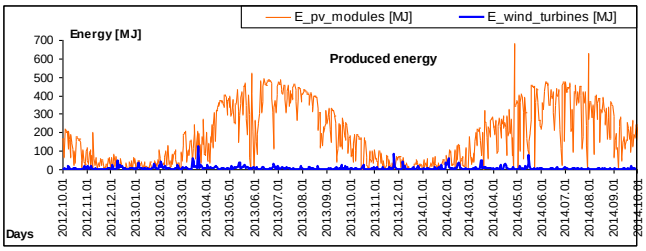

Fig.2. Electrical energy produced by PV modules and wind turbines during the whole period of the project

In Fig.3. the electrical energy consumption of the model house (electrical home appliances, electric heater and air conditioner) is shown in the 2-year period of the project (from 2012-Oct-1 to 2014-Oct-1). The efficiency of resistance heating device is η_{heating}=1, the coefficient of performance of the air conditioner is C_{cooling}=3. The overall heat transmission coefficient of insulated walls is U=0.18 W•m^{-2}•K^{-1}; the emissivity of the building's walls is ε=0.12.

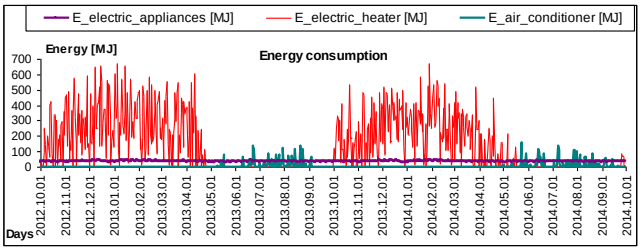

Fig.3. Electrical energy consumption of the house (electric home appliances, electric heater and air conditioner) during the whole period of the project

Computer simulations with spreadsheet software were performed in order to determine the necessary capacity of the storage unit [8]. In the simulation with the given data the necessary capacity of the energy storage unit that must be chosen is approx. 45097 MJ in order to prevent blackouts (in order to $E_{\mathrm{acc},i}$ take values only between 0 and $E_{\mathrm{acc\_max}}$) every day in the 2-year period of the project. We got that the capacity of the accumulator system derived from the simulations has a value too large for a real-world storage system. It cannot be realised in the real world in a house.

Without electric heating

Electric heating is the biggest form of energy consumption in the model house. If the electric heating is rejected and fossil fuel (e.g. wood) heating is applied, then the necessary capacity of storage unit is approx. 547.5 MJ according to our simulation. In this case all electric home appliances and even the air conditioner can be used in the model house in the whole period of the project [8]. This storage capacity might be realised (perhaps), but it would be very expensive.

CONCLUSIONS

Students had to consider some properties of a stand-alone house with a hybrid wind–solar power generator and accumulator system. The parameters of the model house and the dimensions of the hybrid wind-solar power generator system are fitted to data collected by students. Discrete energy balance equations were given to determine the necessary capacity of the energy storage unit. We think that this student project helps to strengthen connection between theory and practice, improving practice within the field of physics education. We hope that this simplified model can be profitable for interested students in grammar schools.

ACKNOWLEDGMENTS

I would like thank Gyula Bene and Tamás Tél (my supervisors) who helped me with useful information and data. I would like to thank my colleagues Orsolya Pap and Antal Fekete, and our students for their contribution to the project.

REFERENCES

1. J. L. Sawin et al.: in: *Renewable Energy Policy Network for the 21st Century, Renewables 2013: Global Status Report* (ed. L. Mastny), Sunna Research and Worldwatch Institute, REN21 Secretariat, Paris, France, 2013
2. D. J. C. Mackay: *Sustainable Energy – without the hot air,* UIT Cambridge, Cambridge England, 2008
3. M. Z. Jacobson and M. A. Delucchi: A Path to Sustainable Energy by 2030, Sci. Am. **301** 58–65, 2009
4. M. Blasone, F. Dell'Anno, R. De Luca and G. Torre: A simple mathematical description of an off-grid hybrid solar–wind power generating system, Eur. J. Phys. **34** 763-71, 2013
5. A. Betz: *Introduction to the Theory of Flow Machines.* Oxford: Pergamon Press, 1966
6. R. De Luca and P. Desideri: Wind energy: an application of Bernoulli's theorem generalized to isentropic flow of ideal gases, Eur. J. Phys. **34**, 189–97, 2013
7. Á. Budó: *Experimental Physics I*, Nemzeti Tankönyvkiadó, Budapest, 1997 (in Hungarian)
8. T. Beke: A simple model for the energy supply of a stand-alone house using a hybrid wind–solar power system. Eur. J. Phys. **37**, 015804, 1–19, 2016

RASPBERRY SOLAR CELL, A VERSATILE TOOL IN TEACHING PHYSICS

Z. Csernovszky[1], Á. Horváth[2]
[1] Kölcsey Secondary School, Budapest, Hungary, csernozoli@gmail.com
Physics Education PhD program, Eötvös University, Budapest
[2]ELTE, Department of Atomic Physics, Budapest, Hungary, akos@ludens.elte.hu

ABSTRACT

The article describes the realization and teaching application of the raspberry solar cell. We present its components and the electron transports of the raspberry solar cell. The description uses the same four steps, the excitation, the charge separation, the diffusion and the regeneration, as the single n-p junction solar cell, and as the light-dependent reactions of photosynthesis. To strengthen the similarities between these solar energy converters, we underline analogies in energy levels and bands. These analogies offer an interdisciplinary approach in teaching applications. The real situation, the construction of the raspberry solar cell, allows the science teacher to place the notion of energy and the solar energy conversion into an interdisciplinary context. For this reason, we organized student activities around this versatile tool. Here we expose the results of a test, realized by homemade solar cells, sensitized by three organic dyes, exposed to different light sources.

RASPBERRY SOLAR CELL

A raspberry solar cell is a dye-sensitized solar cell composed of an anode, a cathode and an electrolyte. The construction of a raspberry solar cell is an interesting project work, but it requires special coated glass plates, laboratory materials, special equipment and preparations for the physics teacher. See needed materials and steps to follow with more references in [1].

The anode consists of a transparent glass plate covered by a semi-conductor layer (Fluorine doped Tin-Oxide or FTO). On this plate, we stabilized a porous, wide bandgap semiconductor (titanium-dioxide or TiO_2) layer. According to its wide bandgap, the semiconductor layers are insensitive to visible light. To prepare a light-sensitive anode, we fixed raspberry dyes (anthocyanin molecules) on the TiO_2 layer. On one hand, this combination of semiconductor layers and raspberry dye layer allows increasing the effective surface of solar cell. On the other hand, the difference between the conduction bands of FTO and of TiO_2 results electrons on the FTO glass plate. The energy of the captured photons excites the electrons (of anthocyanin molecules), which follow the energetically suitable way to the FTO layer.

As cathode, we used another transparent FTO coated glass plate, covered with a carbon layer. This layer acts as a photo-reflecting layer and a catalyst of the electrolyte regeneration. Between these two electrodes, a regenerative electrolyte (iodide/tri-iodide) solution closes the circuit. The solar cell is ready to convert the photon's energy [2].

The left panel of Fig.1. shows the simplified structure of a raspberry solar cell. The right panel presents a homemade raspberry solar cell. The anode side is beige, because TiO_2 is white, the raspberry juice is red, the electrolyte is brown and mixing these colours results in beige. The carbon on the cathode side is black.

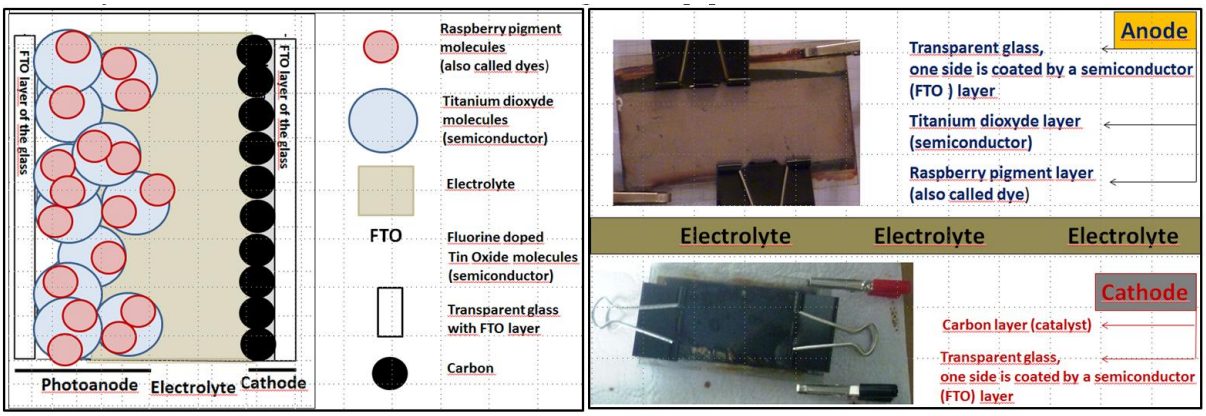

Fig.1. Structure of a raspberry solar cell. Components of a homemade raspberry solar cell

HOW IT WORKS

Due to the internal structure, the unit is a galvanic cell, and it works in dark as well. If we expose the anode side to light, first a ground state raspberry dye molecule absorbs a photon. The excited dye molecule injects an electron into the TiO_2 grain (crystal), at the point where the TiO_2 adsorbed the raspberry dye. This step is the charge separation. After that, the electrons diffuse to the FTO from the TiO_2 layer. Connecting a voltmeter between the electrodes, it measures a voltage. See the left panel of Fig.2.

If we connect the electrodes using an ammeter, it measures an electric current. The electron travels through the outer circle, reaches the cathode, and regenerates the electrolyte and the dye in two steps, as the right panel of Fig.2 shows [3].

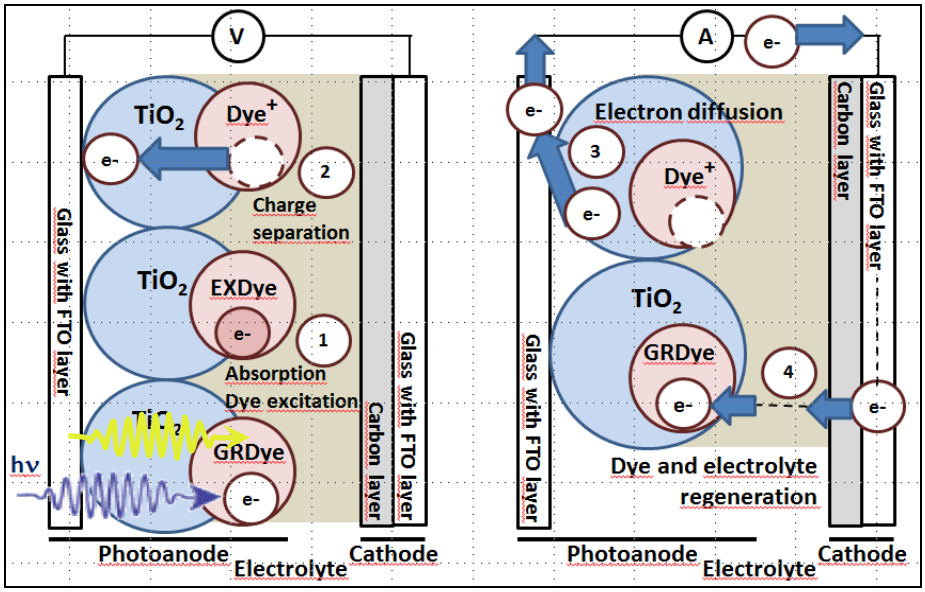

Fig.2. Photovoltaic effect Electric current

One can follow the energy of an electron on the left panel of Fig.3, where we represent the relative energy levels and bands [4]. On the abscissa, there are the components of a cell in spatial order, starting with the place of the photon absorption (Dye). Here the excited state level (EX) is energetically the highest level. The four main steps of an electron-cycle are numbered on the figure. The right panel of Fig.3. represents the components as they are in space. The most absorbed photons, absorbed by the pair TiO_2 – raspberry dye, are the photons of 2.3 eV. See the main steps of an electron-cycle in Table 1 and [5].

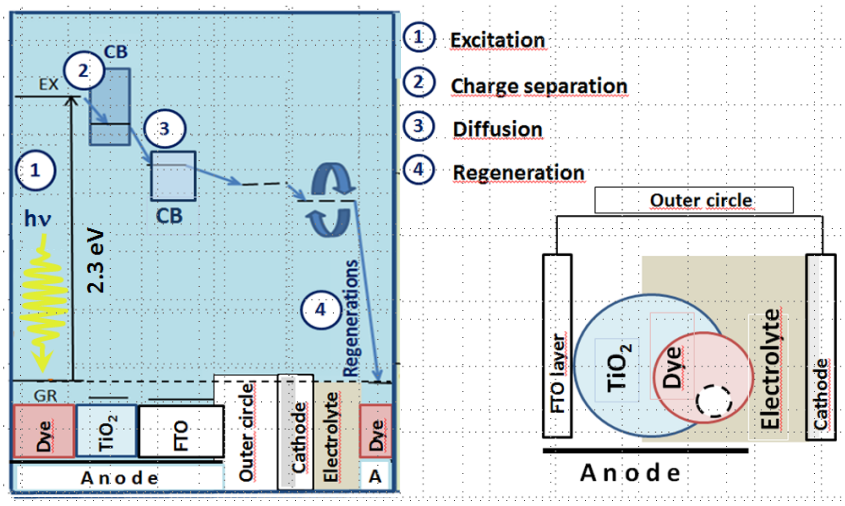

Fig.3. Raspberry solar cell: Relative energy levels and bands Actual order in space

Table 1. Main steps of an electron-cycle of the raspberry solar cell

Steps	Raspberry Solar Cell	GRDye = ground state dye EXDye = excited state dye I^- = iodide / I^-_3 = tri-iodide $e^-_{TiO2,CB}$ = electron in the conduction band of TiO_2 $e^-_{FTO,CB}$ = electron in the conduction band of FTO
1	$GRDye + h \cdot \upsilon \rightarrow EXDye$	
2	$EXDye \rightarrow e^-_{TiO2,CB} + Dye^+$	
3	$e^-_{TiO2,CB} \rightarrow e^-_{FTO,CB}$	
4	Electrolyte: $I_3^- + 2e^- \rightarrow 3I^-$	
	Dye: $2\,Dye^+ + 3I^- \rightarrow 2GRDye + I_3$	

ANALOGIES AND SIMPLIFICATION I. – TEACHING SOLAR CELLS

In practice, most solar cells use semiconductors in the form of an n-p junction, which is formed by joining an n-type and a p-type semiconductor. Near the junction, in the depletion region, a photon's absorption results in an electron-hole pair. Both the electron and the hole can participate in conduction. After the diffusion to the n-type semiconductor, the electron travels through the outer circle and will recombine with a hole, which travels in the opposite direction and diffuse to the p-type semiconductor (see Fig.4.).

In a single n-p junction solar cell, an electron follows the same four main steps as in the raspberry solar cell. In the raspberry solar cell, the excitation and the charge separation steps are spatially divided, which simplifies the description. Here only the electron moves, because the positive dyes (Dye+) are adsorbed on the TiO_2 layer. These facts result in a simplified and localizable electron-cycle. Applying this analogy to the electron- and hole-cycle of a solar cell, the students can understand the basis of solar cells physics. See Fig.5. and Table 2.

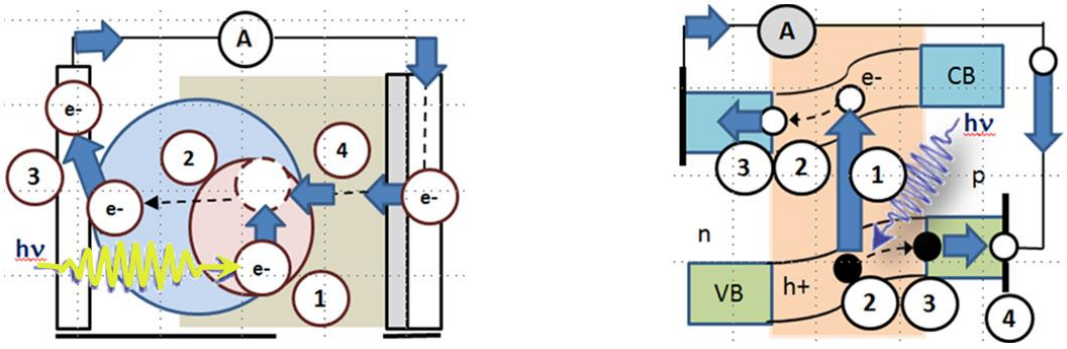

Fig.4. Raspberry solar cell: electron-cycle n-p junction solar cell: electron/ hole cycle

Table 2. Main steps of an electron-hole pair cycle of the n-p junction solar cell

Steps	n-p junction solar cell	e^- = electron in the depletion h^+ = hole in the depletion VB = valence band of depletion CB = conduction band of depletion AC = atomic core SC = semiconductor n /p = n- /p-type semiconductor
①	$e^-_{VB} + h \cdot \upsilon \rightarrow e^-_{CB}$	
②	$e^-_{VB} + AC \rightarrow e^-_{CB} + h^+_{VB}$	
③	e^-: Depletion→ n-typeSC$_{CB}$	
	h^+: Depletion → p-typeSC$_{VB}$	
④	e^- / h^+ recombination: $e^-_{CB} + h^+_{VB} \rightarrow e^-_{VB} + AC^+_{VB}$	

The comparison of the energy bands of the two types of solar cells shows that the raspberry solar cell has a simplified energy band structure because of the immobility of the dyes and of the localized steps of a cycle on the different components of the cell. On the n-p junction solar cell, the student has to follow the energy of the electron and of the hole, and has to understand the deformed energy structure of the depletion region, too.

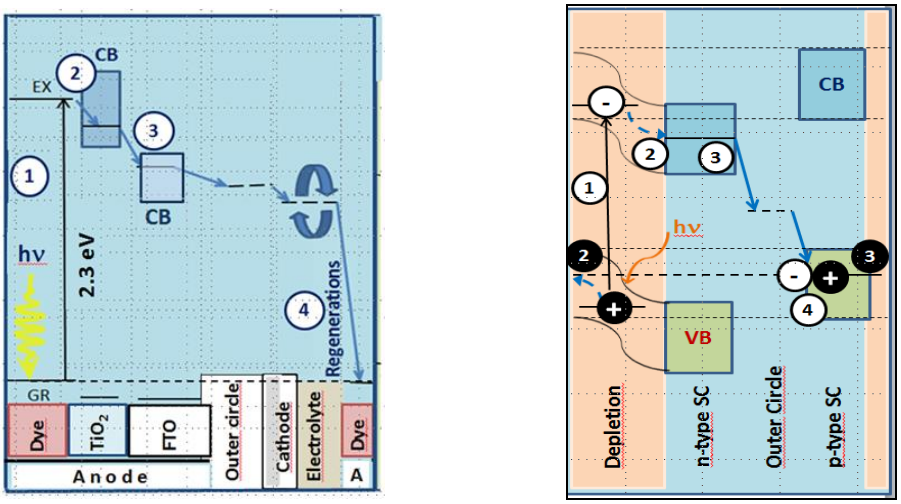

Fig.5 Raspberry solar cell: relative energy bands, n-p junction solar cell: relative energy bands

TEST OF A HOMEMADE RASPBERRY SOLAR CELL

After the realization, we used the raspberry solar cell as a galvanic cell, and we measured the voltage in dark. In use, the current supplied by the solar cells is important, and determines the electric power taken from them. We used different light sources (bulb, neon, halogen, LED, UV) and different dyes (raspberry-, blueberry- and mango dyes) to measure the generated current.

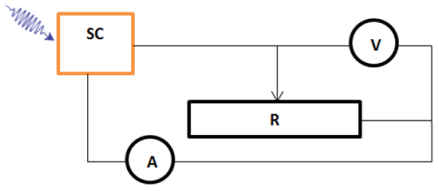

Fig.6. Solar cell as current source

For a comparative analysis of raspberry- and n-p junction solar cells, we used illuminated cells as current source in the electrical circuit of Fig.6, where we connected a variable resistor. We measured its voltage (V) and current (I) at same time. We found a linear dependence according to Ohm's law of the circuit ($V=V_0-R_{internal} \cdot I$), then we determined the internal resistances (R_i) and the electromotive forces (V_0) of the cells. For example, applying an UV light-source for raspberry cell, we measured a dependence V(mV)=60- 0.17·I(μA), by which

R_i=170 Ω, V_0=60 mV. For a commercial garden lamp, composed of n-p junction solar cells, we measured V(mV)=2471-307 I(mA), by which R_i=307 Ω, V_0=2471 mV.

We determined the maximal power output of the cells, on one hand using Ohm's law of the circuit ($P= (V_0-R_i \cdot I) \cdot I$), on the other hand analysing power-current functions. We defined the quotient $|P_{Ohm}-P_{function}| / P_{Ohm}$ as the relative power error. The test of the raspberry cell using an UV light-source, gives 7% optimal power relative errors. With the same light source, the relative power error for solar cell garden lamp was 12%. See Fig.7 and more test results in [6].

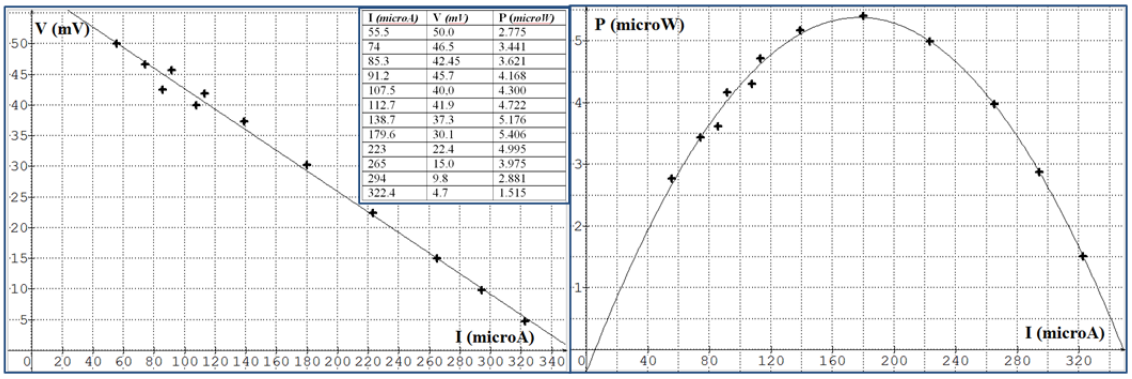

Voltage as function of current Power as function of current

Fig.7. Solar cells as current source, illuminated by UV light-source

ANALOGIES AND SIMPLIFICATION II. - TEACHING PHOTOSYNTHESIS

The raspberry cell uses the same basic principle as plant photosynthesis to generate electricity from sunlight. Both processes require the absorption of the energy of photons. In the cycle of light dependent reactions of the photosynthesis, the electron follows the four main steps twice: excitation, charge separation, diffusion and regeneration.

The right panel of Fig.8 presents the absorptions of two photons of different frequencies, and that the linear electron transport chain connects the two parts of light dependent reactions, the photosystems I and II. Photolysis, the regeneration process in this case, with the electron replacement results in a cyclic operation.

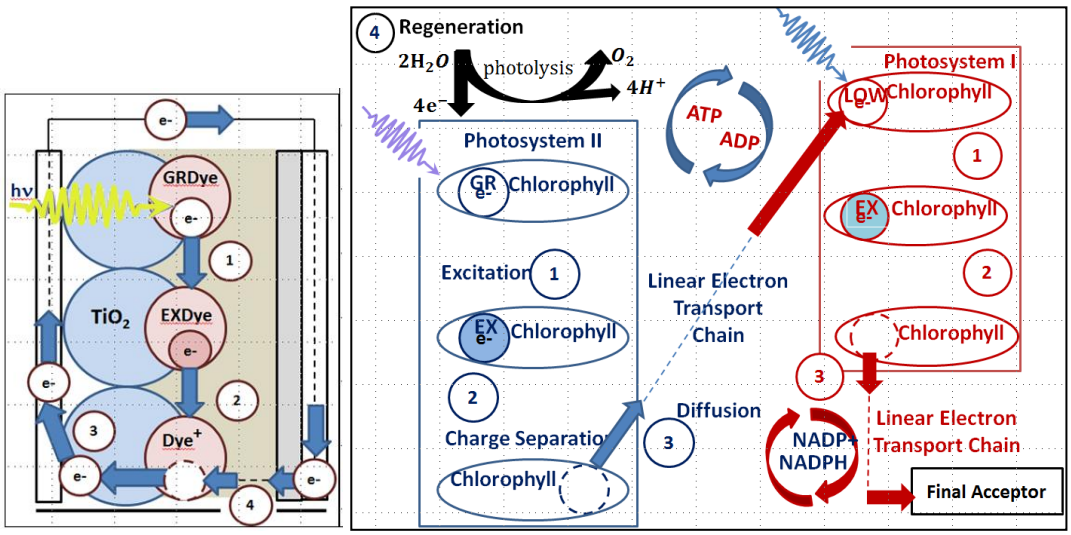

Fig.8. Electron-cycles: Raspberry cell Light dependent reactions of photosynthesis

From the point of view of physics teaching, a comparative analysis of relative energy bands and levels underline the similarities of the two processes, in spite of the electron-cycle repeating twice. On Fig.9, we compared how different parts of a raspberry cell and of light dependent reactions use the energies of the photons. (For more details see [4], [5] and [7].)

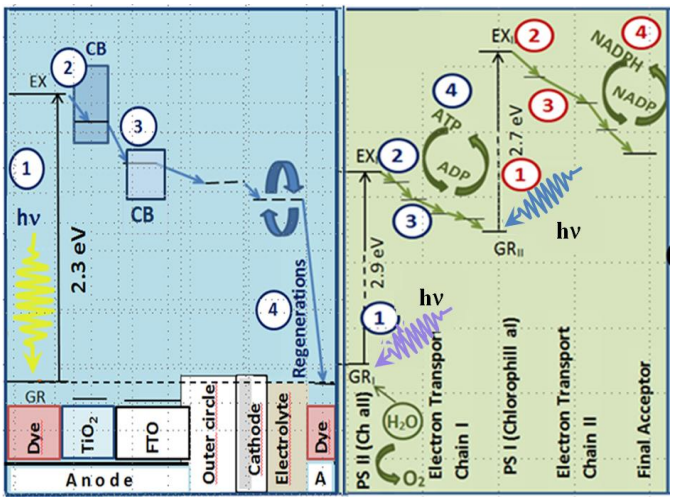

Fig.9. Raspberry cell: relative energy levels LDR of photosynthesis: relative energy levels

With the relatively simple energy cycle and energy band structure the raspberry cell can illustrate many different scientific subjects, like galvanic cells, semiconductors, n-p junction solar cells, light-dependent reactions of photosynthesis, current sources. Placing the energy concept into an interdisciplinary context can offer an understanding and integration of many different pre-existing concepts. It can help in the description of all types of solar energy converters, and in many issues of environmental sciences [8].

CONCLUSIONS

The raspberry solar cell works according to the same basic principle as other photovoltaic and galvanic systems. Based on this fact, physics curriculum and teaching objectives can utilize this analogy during physics teaching at several levels. We presented a short introduction of two possible analogies. We examined the electron cycles and the energy levels analogies, starting from the raspberry cell case and moving to the more complex photosynthesis and semiconductor solar cell cases.

We underlined that the teacher can organize physics, chemistry and biology class activities around the raspberry solar cell. We described here the steps to build a raspberry cell, even though we recommend the do-it-yourself method only to upper secondary classes, in the presence of a teacher, with prepared glass plates and electrolyte. To demonstrate its function and discover it in action, we tested the effects of light-sources and of different dyes on the cell. Finally, we used the cell as current source to compare to an n-p junction solar cell [1],[6].

REFERENCES

1. Build a raspberry cell: http://fr.calameo.com/read/00004272704000f5bfeb0
2. Grätzel, M., Photoelectrochemical cells. Nature **414**, 338–344 (2001)
3. Khan, Z. N., Study on Optimization of Dye Sensitized Solar Cells. Thesis, University of South Florida, 2013
4. Le Bahers, T., Optimisation des cellules solaires a colorants a base de ZnO par une approche combinéee théorie/expérience. These, Université P. et M Curie, Paris VI, 2011
5. Notes for Fig.3, Fig.8: http://fr.calameo.com/read/000042727c9fa67e36268
6. Test of solar cells: http://fr.calameo.com/read/00004272749e446d4730b
7. Tavernier, R., Biologie, Terminale D, Édition Bordas, 1989 (p.131, Fig.2)
8. Barker, M., Carr, M., Teaching and learning about photosynthesis. International Journal of Science Education, 11(1), 49–56 (1989)

Refs. 1., 5., 6. are published by the authors.